JGP Journal of General Physiology

RESEARCH ARTICLE

Binding and structural asymmetry governs ligand sensitivity in a cyclic nucleotide–gated ion channel

Leo C.T. Ng[1], Meiying Zhuang[1], Filip Van Petegem[2], Yue Xian Li[3], and Eric A. Accili[1]

Hyperpolarization-activated cyclic nucleotide-gated (HCN) channels open more easily when cAMP or cGMP bind to a domain in the intracellular C-terminus in each of four identical subunits. How sensitivity of the channels to these ligands is determined is not well understood. Here, we apply a mathematical model, which incorporates negative cooperativity, to gating and mutagenesis data available in the literature and combine the results with binding data collected using isothermal titration calorimetry. This model recapitulates the concentration–response data for the effects of cAMP and cGMP on wild-type HCN2 channel opening and, remarkably, predicts the concentration–response data for a subset of mutants with single-point amino acid substitutions in the binding site. Our results suggest that ligand sensitivity is determined by negative cooperativity and asymmetric effects on structure and channel opening, which are tuned by ligand-specific interactions and residues within the binding site.

Introduction

Hyperpolarization-activated cyclic nucleotide-gated (HCN) channels are activated by hyperpolarization of the membrane potential, and most isoforms open more easily when cAMP binds to a cyclic nucleotide binding domain (CNBD) located in the intracellular C-terminus (DiFrancesco and Tortora, 1991; Gauss et al., 1998; Ludwig et al., 1998; Santoro et al., 1998). Current functional evidence in the HCN2 channel suggests that cAMP binding relieves tonic inhibition of the pore by an intracellular C-terminal region of HCN2 made up of the CNBD and a domain called the C-linker connecting the CNBD to the pore (Wainger et al., 2001). The structure of this CNBD and C-linker region of the HCN2 isoform was solved by x-ray crystallography in cyclic nucleotide–bound and unbound states, and it is a symmetrical tetramer (Zagotta et al., 2003; Taraska et al., 2009; Ng et al., 2016). A recent cryo-EM structure of the HCN1 isoform confirms that the channel is a symmetrical tetramer and also shows that the C-linker/CNBD regions, hanging below the pore, adopt a structure that is similar to the solved structure of the HCN2 C-terminus (Lee and MacKinnon, 2017).

Studies using transition ion metal FRET, double electron-electron resonance, and NMR have suggested that cAMP binding to the HCN2 and HCN4 C-terminal regions shifts the B- and C-helices of the CNBD toward the β-roll, and that the secondary structures of the P- and C-helices become more stable (Taraska et al., 2009; Puljung and Zagotta, 2013; Puljung et al., 2014; Saponaro et al., 2014; Akimoto et al., 2014; Akimoto et al., 2018). The recent cryo-EM structure of the HCN1 isoform, which is as sensitive to cAMP as the HCN2 isoform but in which the maximum effect is less (Wang et al., 2001), in the bound and unbound conformation, showed similar alterations in single subunits but also demonstrated a right-handed rotation of the CNBD and C-linker of all subunits relative to the pore and other transmembrane domains (Lee and MacKinnon, 2017).

In most HCN forms, submicromolar levels of cAMP facilitate opening by shifting the activation curve to less negative voltages (DiFrancesco and Tortora, 1991). For the mammalian HCN2 isoform, 50% effective concentration (EC_{50}) values determined by the Hill equation were found to be ∼0.1 µM for cAMP, with a maximum depolarizing shift of the activation curve of ∼18 mV and a Hill coefficient of ∼1 (Wang et al., 2001; Zagotta et al., 2003; Flynn et al., 2007; Zhou and Siegelbaum, 2007). The EC_{50} values are ≥10 times larger for cGMP than for cAMP, even though both cyclic nucleotides, at saturating levels, produce the same maximum depolarizing shift in activation (Wang et al., 2001; Zagotta et al., 2003; Flynn et al., 2007; Zhou and Siegelbaum, 2007). It is not known if the difference in potency (defined as the EC_{50} value) between cAMP and cGMP is due to a difference in binding affinity (defined as the dissociation constant, K_d) to the channel or how strongly binding is coupled to pore opening (Colquhoun, 1998). Understanding the molecular basis of this difference is important, because cGMP could effectively compete with cAMP for binding

[1]Department of Cellular and Physiological Sciences, University of British Columbia, Vancouver, BC, Canada; [2]Department of Biochemistry and Molecular Biology, University of British Columbia, Vancouver, BC, Canada; [3]Department of Mathematics, University of British Columbia, Vancouver, BC, Canada.

Correspondence to Eric A. Accili: eaaccili@mail.ubc.ca.

in vivo if the difference in potency between these molecules were mainly due to differences in how binding is coupled to opening rather than to differences in binding affinity.

Despite the studies performed to date, how cyclic nucleotides facilitate opening and how sensitivity of HCN channels to these ligands is determined, at the molecular and atomistic levels, is not well understood. A major challenge for understanding ligand sensitivity of pore opening in ligand-gated ion channels, including HCN channels, is to obtain a relevant measure of binding affinity directly by experiment (Colquhoun, 1998; Hines et al., 2014). We have developed an approach using isothermal titration calorimetry (ITC) to determine the affinity of cAMP for a freely occurring tetrameric form of the HCN2 C-terminus fragment containing the CNBD and C-linker (Chow et al., 2012; Ng et al., 2016). This C-terminus region is comprised of six α-helices in the C-linker and the four α-helices and eight β-strands that constitute the CNBD, and is identical to that solved by x-ray crystallography (Zagotta et al., 2003). By ITC, we found that cAMP binding proceeds with negative cooperativity to the tetrameric CNBD; binding of one cAMP occurred to one subunit with high affinity (K_d ~0.1 μM) and subsequent binding of three cAMP molecules to the remaining subunits with lower affinity (K_d ~1.5 μM; Chow et al., 2012; Ng et al., 2016). This is surprising, because concentration–response data for the effect of cAMP on the full-length HCN2 channel activation curve, when fitted with the Hill equation, yield Hill coefficients of ~1. Finally, cGMP may also bind to this structure with negative cooperativity, with K_d values of ~0.4 and ~8.5 μM for the high- and low-affinity binding events, respectively (Ng et al., 2016). The high-affinity binding of cGMP occurs in a range of concentrations that might be expected normally in vivo.

We also found that binding of cAMP and cGMP to the HCN2 C-terminal tetramer was accompanied by a distinct and asymmetric thermodynamic signature, which showed that the high-affinity binding event is associated with favorable entropy and favorable enthalpy, whereas the lower-affinity event is associated with favorable enthalpy but with unfavorable entropy (Chow et al., 2012; Ng et al., 2016). Furthermore, the enthalpic component of low-affinity binding is even larger than that for high-affinity binding. Thus, the thermodynamic basis for negative cooperativity is entirely entropic. It is notable that this binding asymmetry arises despite the fourfold symmetry observed in the solved structures of the HCN1 and HCN2 channels.

To understand how ligand sensitivity is determined at the molecular level and arises from negative cooperativity, we have used experimental binding and gating data to develop a mathematical model for the concentration dependence of the ligand-induced shift of HCN2 channel opening to less negative voltages. Our experimental and modeling results are consistent with an asymmetric model for cyclic nucleotide facilitation of HCN2 channel opening.

Materials and methods

A mathematical model for the shift in HCN2 channel opening to less negative voltages

Here, we developed a steady-state model for the depolarizing shift in the activation curve produced by cAMP by using the Boltzmann equation with a slope that is unaltered by cAMP, as shown previously by experiment (Chen et al., 2001). To fit with experimental data, we develop the model in progressive steps, starting with the case when the cAMP binding sites in three of four subunits are blocked, leaving only one binding site available in each channel molecule. In this case, the model is described by the following schematic diagram.

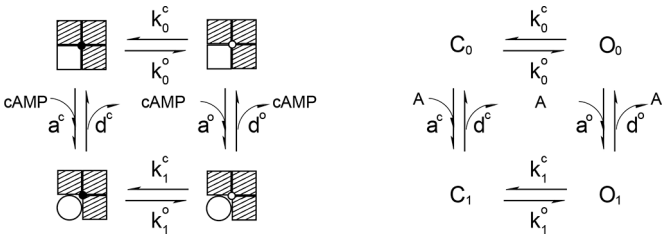

(Scheme 1)

A shaded square represents a subunit on which the cAMP binding is blocked, while an open square represents a subunit on which the cAMP binding is not blocked. The open circle stands for a subunit that is already bound by cAMP. The filled small circle in the center represents that the channel is in a closed state while an open small circle represents that the channel is in an open state. k_j^o, k_j^c are the rate constants of channel opening and closing, respectively, when the channel is bound with j cAMP molecules. Thus, the subscript j represents the number of cAMP molecules bound to each channel state. j = 0,1 in the present case and j = 0,1,2,3,4 in the full model that we shall present later. $a^s$and d^s are, respectively, the association (binding) and dissociation (unbinding) rate constants of cAMP to a channel in state s. Therefore, the superscript s represents a channel in a closed ($s = c$) or an open ($s = o$) state.

In the reaction scheme on the right, a channel in open and closed state are represented, respectively, by the letters O_j and C_j. Again, the subscript j is the number of cAMP molecules bound to the channel. cAMP is abbreviated by letter A to make the diagram less busy.

In the absence of cAMP, only the top two states exist. At steady-state,

$$k_0^o[C_0] = k_0^c[O_0] \Rightarrow \frac{[O_0]}{[C_0]} = \frac{k_0^o}{k_0^c} = 1. \quad (1)$$

This is because, in the Boltzmann expression of channel opening (below)

$$f_o = \left[1 + \exp\left(\frac{V - V_h}{q}\right)\right]^{-1},$$

we assume, for convenience, that voltage is fixed at $V = V_h$ or f_o = 0.5 (i.e., $[O_0] = [C_0]$) in the absence of cAMP. Therefore, $k_0^o = k_0^c = k_0$ in our study. We use square brackets to represent the number of channels in each state. It is straightforward to write down the differential equations governing the time evolution of the four channel states. However, they must satisfy the constraint $[T] = [C_0] + [C_1] + [O_0] + [O_1]$ = constant.

Assuming that cAMP binding is much faster than the change in structure associated with channel opening and closing, we have

$$k_j^c, k_j^o \ll a^c, a^o, d^c, d^o, \quad (j = 0, 1). \tag{2}$$

Therefore, we expect cAMP binding to reach a steady state much faster than do channel opening and closing:

$$\begin{aligned} a^c[A][C_0] = d^c[C_1] \Rightarrow [A][C_0] = K^c[C_1] \\ a^o[A][O_0] = d^o[O_1] \Rightarrow [A][O_0] = K^o[O_1], \end{aligned} \tag{3}$$

where $K^c = d^c/a^c, K^o = d^o/a^o$ are, respectively, the dissociation constants for the closed and the open channels. Now, let's introduce the numbers of channels in closed and open states, respectively:

$$\begin{aligned} [C] = [C_0] + [C_1] = [C_0] + \frac{[A]}{K^c}[C_0] = \\ \left(1 + \frac{[A]}{K^c}\right)[C_0] \Rightarrow [C_0] = \frac{1}{1 + \frac{[A]}{K^c}}[C] \\ [O] = [O_0] + [O_1] = [O_0] + \frac{[A]}{K^o}[O_0] = \\ \left(1 + \frac{[A]}{K^o}\right)[O_0] \Rightarrow [O_0] = \frac{1}{1 + \frac{[A]}{K^o}}[O]. \end{aligned} \tag{4}$$

Similarly,

$$\begin{aligned} [C_1] = [C] - [C_0] = \frac{\frac{[A]}{K^c}}{1 + \frac{[A]}{K^c}}[C] \\ [O_1] = [O] - [O_0] = \frac{\frac{[A]}{K^o}}{1 + \frac{[A]}{K^o}}[O]. \end{aligned} \tag{5}$$

Knowing that $[T] = [C] + [O]$ is a constant, we can write down the differential equation governing the time evolution of $[O]$, which yields the following steady-state fraction of open channels:

$$F = \frac{[O]_s}{[T]} = \frac{L_o}{L_o + L_c}, \tag{6}$$

where

$$L_o^{(1)} = k_0^o \frac{1 + \kappa^o \frac{[A]}{\kappa^c}}{1 + \frac{[A]}{\kappa^c}}$$

and

$$L_c^{(1)} = k_0^c \frac{1 + \kappa^c \frac{[A]}{\kappa^o}}{1 + \frac{[A]}{\kappa^o}}, \quad \left(\kappa^o = \frac{k_1^o}{k_0^o}, \ \kappa^c = \frac{k_1^c}{k_0^c}\right) \tag{7}$$

are, respectively, the rate constants of channel opening and closing in the presence of cAMP at the dose of $[A]$.

The Boltzmann expression of the HCN activation curve is

$$f_0(V) = \frac{1}{1 + \exp\left(\frac{V - V_h}{q}\right)}. \tag{8}$$

Here, V is the test voltage (mV), V_h is the half-activation voltage (mV), and q is the slope factor (mV).

Let $\Delta V > 0$ be the shift of the activation curve induced by the addition of cAMP; thus the shifted curve is described by

$$f(V) = \frac{1}{1 + \exp\left(\frac{V - V_h - \Delta V}{q}\right)}. \tag{9}$$

At $V = V_h$,

$$\begin{aligned} F = f(V_h) = \frac{1}{1 + \exp\left(\frac{-\Delta V}{q}\right)} \Rightarrow \exp\left(\frac{-\Delta V}{q}\right) \\ = \frac{1}{F} - 1 = \frac{1 - F}{F} = \frac{L_c}{L_o}. \end{aligned} \tag{10}$$

Therefore,

$$\Delta V([A]) = q\ln\left(\frac{L_o^{(1)}}{L_c^{(1)}}\right) = q\ln\left(\frac{k_0^o}{k_0^c} \frac{\frac{1 + \kappa^o \frac{[A]}{K^c}}{1 + \frac{[A]}{K^c}}}{\frac{1 + \kappa^c \frac{[A]}{K^o}}{1 + \frac{[A]}{K^o}}}\right). \tag{11}$$

Immediate predictions are, for $[A] = 0$,

$$\Delta V_0 = \Delta V(0) = q\ln\left(\frac{k_0^o}{k_0^c}\right) = q\ln(1) = 0. \tag{12}$$

For $[A] = \infty$,

$$\Delta V_m = \Delta V(\infty) = q\ln\left(\frac{\kappa^o}{\kappa^c}\right) = q\ln(K_1), \quad \left(K_1 = \frac{\kappa^o}{\kappa^c} = \frac{k_1^o}{k_1^c}\right). \tag{13}$$

Therefore, if $\Delta V_m > 0, K_1 > 1$, i.e., $k_1^o > k_1^c$ is necessary to guarantee a positive shift. In other words, to achieve a positive shift, the binding of cAMP to a channel must result in higher channel opening rate compared with channels that are not bound with cAMP.

The model may be extended to the case where the cAMP binding sites on two subunits are available, shown schematically below.

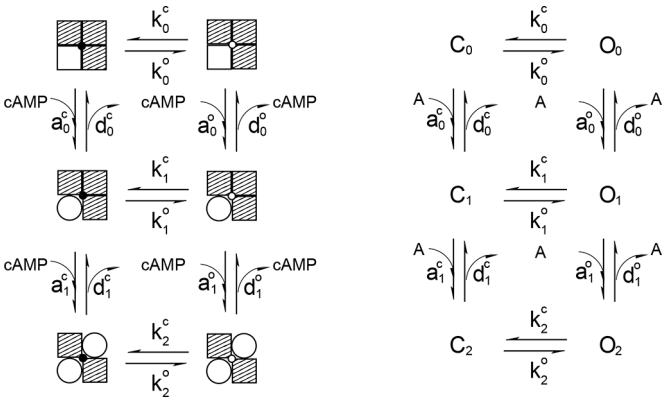

(Scheme 2)

Following the calculations similar to those described above, we found that

$$L_o^{(2)} = \frac{\Gamma^o}{J^c} = \frac{k_0^o + k_1^o\frac{3[A]}{K_0^c} + k_2^o\frac{3[A]^2}{K_0^cK_1^c} + k_3^o\frac{[A]^3}{K_0^cK_1^cK_2^c}}{1 + \frac{3[A]}{K_0^c} + \frac{3[A]^2}{K_0^cK_1^c} + \frac{[A]^3}{K_0^cK_1^cK_2^c}}, \quad (14)$$

$$L_c^{(2)} = \frac{\Gamma^c}{J^o} = \frac{k_0^c + k_1^c\frac{3[A]}{K_0^o} + k_2^c\frac{3[A]^2}{K_0^oK_1^o} + k_3^c\frac{[A]^3}{K_0^oK_1^oK_2^o}}{1 + \frac{3[A]}{K_0^o} + \frac{3[A]^3}{K_0^oK_1^o} + \frac{[A]^3}{K_0^oK_1^oK_2^o}}. \quad (15)$$

Likewise, when all four subunits are available for cAMP binding, we obtain

$$L_o^{(4)} = \frac{\Gamma^o}{J^c} = \frac{k_0^o + k_1^o\frac{4[A]}{K_0^c} + k_2^o\frac{6[A]^2}{K_0^cK_1^c} + k_3^o\frac{4[A]^3}{K_0^cK_1^cK_2^c} + k_4^o\frac{[A]^4}{K_0^cK_1^cK_2^cK_3^c}}{1 + \frac{4[A]}{K_0^c} + \frac{6[A]^2}{K_0^cK_1^c} + \frac{4[A]^3}{K_0^cK_1^cK_2^c} + \frac{[A]^4}{K_0^cK_1^cK_2^cK_3^c}}, \quad (16)$$

$$L_c^{(4)} = \frac{\Gamma^c}{J^o} = \frac{k_0^c + k_1^c\frac{4[A]}{K_0^o} + k_2^c\frac{6[A]^2}{K_0^oK_1^o} + k_3^c\frac{4[A]^3}{K_0^oK_1^oK_2^o} + k_4^c\frac{[A]^4}{K_0^oK_1^oK_2^oK_3^o}}{1 + \frac{4[A]}{K_0^o} + \frac{6[A]^3}{K_0^oK_1^o} + \frac{4[A]^3}{K_0^oK_1^oK_2^o} + \frac{[A]^4}{K_0^oK_1^oK_2^oK_3^o}}. \quad (17)$$

In the expressions above, the dissociation constants are defined as

$$K_j^s = \frac{d_j^s}{a_j^s}, \quad (s = c, o; j = 0, 1, 2, 3). \quad (18)$$

Introducing dimensionless quantities,

$$\kappa_i^c = \frac{k_i^c}{k_0^c}, \kappa_i^o = \frac{k_i^o}{k_0^o}, \quad (i = 0, 1, 2, 3, 4),$$

thus $\kappa_0^o = \kappa_0^c = 1$ and

$$\alpha_c = \frac{[A]}{K_0^c}, \alpha_c^2 = \frac{[A]^2}{K_0^cK_1^c}, \alpha_c^3 = \frac{[A]^3}{K_0^cK_1^cK_2^c}, \alpha_c^4 = \frac{[A]^4}{K_0^cK_1^cK_2^cK_3^c}, \quad (19)$$

$$\alpha_o = \frac{[A]}{K_0^o}, \alpha_o^2 = \frac{[A]^2}{K_0^oK_1^o}, \alpha_o^3 = \frac{[A]^3}{K_0^oK_1^oK_2^o}, \alpha_o^4 = \frac{[A]^4}{K_0^oK_1^oK_2^oK_3^o}. \quad (20)$$

Therefore,

$$L_o^{(4)} = k_0^o\frac{\kappa_0^o + 4\kappa_1^o\alpha_c + 6\kappa_2^o\alpha_c^2 + 4\kappa_3^o\alpha_c^3 + \kappa_4^o\alpha_c^4}{1 + 4\alpha_c + 6\alpha_c^2 + 4\alpha_c^3 + \alpha_c^4} = k_0^o\frac{\sum_{i=0}^4\kappa_i^oC_i^4\alpha_c^i}{\sum_{i=0}^4C_i^4\alpha_c^i} = k_0^o\frac{1 + \sum_{i=1}^4\kappa_i^oC_i^4\prod_{j=0}^3\alpha_j^c}{1 + \sum_{i=1}^4C_i^4\prod_{j=0}^3\alpha_j^c}, \quad (21)$$

$$L_c^{(4)} = k_0^c\frac{\kappa_0^c + 4\kappa_1^c\alpha_o + 6\kappa_2^c\alpha_o^2 + 4\kappa_3^c\alpha_o^3 + \kappa_4^c\alpha_o^4}{1 + 4\alpha_o + 6\alpha_o^2 + 4\alpha_o^3 + \alpha_o^4} = k_0^c\frac{\sum_{i=0}^4\kappa_i^cC_i^4\alpha_o^i}{\sum_{i=0}^4C_i^4\alpha_o^i} = k_0^c\frac{1 + \sum_{i=1}^4\kappa_i^cC_i^4\prod_{j=0}^3\alpha_j^o}{1 + \sum_{i=1}^4C_i^4\prod_{j=0}^3\alpha_j^o}, \quad (22)$$

where $\alpha_j^c = [A]/K_j^c, \alpha_j^o = [A]/K_j^o, (j = 0, 1, 2, 3)$.

Notice that

$$\frac{k_0^o}{k_0^c} = 1,$$

we have the shift as a function of cAMP concentration for channels with four active binding subunits:

$$\Delta V([A]) = q\ln\left[\frac{L_o^{(4)}}{L_c^{(4)}}\right] = s\ln\left[\frac{\frac{\sum_{i=0}^4\kappa_i^oC_i^4\alpha_c^i}{\sum_{i=0}^4C_i^4\alpha_c^i}}{\frac{\sum_{i=0}^4\kappa_i^cC_i^4\alpha_o^i}{\sum_{i=0}^4C_i^4\alpha_o^i}}\right] = q\ln\left[\frac{\left(\sum_{i=0}^4\kappa_i^oC_i^4\alpha_c^i\right)\left(\sum_{i=0}^4C_i^4\alpha_o^i\right)}{\left(\sum_{i=0}^4\kappa_i^cC_i^4\alpha_o^i\right)\left(\sum_{i=0}^4C_i^4\alpha_c^i\right)}\right]. \quad (23)$$

It is easy to check that, at $[A] = 0$, $\alpha_c^i = \alpha_o^i = 0$ for all $i > 0$. In this case, $\Delta V(0) = 0$. At $[A] = \infty$, which means the saturating levels of cAMP,

$$\Delta V(\infty) = q\ln\left[\frac{\kappa_4^o}{\kappa_4^c}\right] = q\ln\left[\frac{k_4^o}{k_4^c}\right] = q\ln(K_4). \quad (24)$$

Here,

$$K_j = \frac{k_j^o}{k_j^c}, \quad (j = 1, 2, 3, 4) \quad (25)$$

measures the bias between the rate of channel opening and that of channel closing after the channel is bound to j cAMP molecules. Experimental data collected so far seem to suggest that $K_j > 1$ for all $j = 1,2,3,4$. Also, $K_4 > K_3 > K_2 > K_1$.

In other words, binding of cAMP to the channel always facilitates the opening of the channel. The more cAMP molecules are bound, the higher the ratio between the opening rate and the closing rate. Therefore, more cAMP binding results in stronger bias toward channel opening.

We did not apply detailed balance to the model because, in the experiments measuring activity and the effect of cyclic nucleotides in excised patches, we consider the channels to have reached a nonequilibrium steady state and not thermodynamic equilibrium.

Molecular biology and cloning

The HCN2 template used previously (Chow et al., 2012), which spans amino acid residues 443–645 and includes the C-linker and CNBD, was excised and inserted in a pET28 vector, with a HMT (hexahistidine, maltose binding protein, and tobacco-etch virus cleavage site) tag in the N-terminus of the construct. Single point mutations were made using PCR and specific sets of primers following the Quikchange protocol (Strategene). The mutated constructs were confirmed by sequencing before expressing in Rosetta DE3 pLacI cells. Cells were induced by 0.4 M isopropyl-β-D-thiogalactoside and harvested after 4 h.

Protein purification

Protein purification was performed as described previously (Chow et al., 2012; Ng et al., 2016). Harvested cells were resolubilized in lysis buffer, lysed by sonication, and centrifuged to release the fusion protein to supernatant as described previously. The fusion protein bound to TALON cobalt affinity column (Clontech) and was eluted by imidazole. The HMT tag

was cleaved by tobacco-etch virus so that the cleaved HCN C-terminus protein would flow through the cobalt column. Finally, the C-terminus was purified by a Resource S cation exchanger (GE Healthcare) and eluted with an increasing [KCl] gradient, at pH 6.0 and 4°C. Protein was dialyzed in 150 mM KCl, 20 mM HEPES, pH 7.0, and 10 mM β-mercaptoethanol. Purity was confirmed with SDS-PAGE, and concentration were determined by spectrophotometry and the Edelhoch method.

Isothermal titration calorimetry

ITC was performed as described previously (Chow et al., 2012). cAMP or cGMP (2 mM) was titrated, 1 µl at a time, into the sample cell containing 200 µM of respective purified protein constructs (in 300 µl initial volume), for a total of 40 injections. We have shown previously that this concentration of protein forms predominantly tetramers and that negative cooperativity occurs only when the protein is present at concentrations >100 µM and does not likely arise from cAMP-induced oligomerization of the protein (Chow et al., 2012). The mutations do not modify gating in the absence of ligand (Zhou and Siegelbaum, 2007), they are not found at the tetramer interface (Zagotta et al., 2003), and in this study, all except E582A (and R632A) do not eliminate negatively cooperative binding of cAMP. Therefore, we assumed that the mutant proteins were also tetrameric at this concentration. The reference cell contained filtered water. The experiments were performed at 25°C, and the heat difference between the sample and reference cell was recorded upon each injection. At least three replicates were compiled for each protein–ligand combination.

The heat difference at each injection interval was integrated to obtain kilocalories per mole of injectant. Origin 7.0 (with MicroCal ITC add-on) was used to fit the isotherm with either a one- or two-site independent binding model, from which affinity, thermodynamics, and stoichiometry were determined. The models and fitting procedures have been described previously (Leavitt and Freire, 2001; Velázquez-Campoy et al., 2004; Velázquez Campoy and Freire, 2005), are also found in the MicroCal Tutorial Guide, and are presented here briefly.

The binding equations for the one-site model are

$$K_a = \frac{\Theta}{(1-\Theta)[X]}, \tag{26}$$

$$Xt = [X] + n\theta Mt, \tag{27}$$

where K_a is the affinity constant, n is the number of binding sites, Θ is the fraction of sites occupied by the ligand, Mt is the protein concentration, Xt is the total concentration of ligand, and $[X]$ is the free concentration of ligand.

The equation for the total heat content, Q, in the one-site binding model is

$$Q = n\theta Mt\Delta HV, \tag{28}$$

where V is the reaction volume and ΔH is the molar heat of ligand binding.

The equations for the two-site binding model are

$$K_1 = \frac{\Theta_1}{(1-\Theta_1)[X]}, \tag{29}$$

$$K_2 = \frac{\Theta_2}{(1-\Theta_2)[X]}. \tag{30}$$

The equation for the total heat content in the two-site independent binding model is

$$Q = MV(n_1\Theta_1\Delta H_1 + n_2\Theta_2\Delta H_2). \tag{31}$$

In both cases, the binding site equations are solved for Θ, and the result is substituted for Θ in the equations for total heat content. A correction for displaced volume (after completion of the injection) and calculation of the change in heat (ΔQ) by that injection are made, using initial guesses for n, K, and ΔH. This is compared with the measured heat and improved using the Marquardt methods until no further change is noted.

The change in free energy (ΔG) is determined from the value for K, and the change in entropy (ΔS) is determined from the equation

$$\Delta G = \Delta H - T\Delta S. \tag{32}$$

As we mentioned previously (Chow et al., 2012), binding isotherms are described by the equation

$$c = K_a[M]n, \tag{33}$$

where K_a is the association constant, $[M]$ is the total protein concentration in the cell, and n is the stoichiometry of interaction. The value for c was between 1 and 1,000 for most of the data used for this study, which is generally considered to yield data that is accurate (Wiseman et al., 1989). In our study, cGMP binding to the HCN2 R591A and T592A mutants, and cAMP and cGMP binding to the E582A-HMT mutants, yielded c values <1. For these mutants, the low levels of heat and poor affinity make it difficult to extract accurate values from the fitting analysis. Nevertheless, the data suggest large reductions in affinity and support the importance of the interactions between the side chains of these residues for tight binding.

Online supplemental material

Fig. S1 shows that cAMP and cGMP bind to the E582A mutant with reduced affinity and without negative cooperativity compared with their binding to the wild-type HCN2 C-terminus fragment. Fig. S2 shows a summary of the effects of single mutations of residues of the HCN2 cyclic nucleotide binding region on high and low binding affinity of cAMP and cGMP. Fig. S3 is a summary of thermodynamic values for cAMP and cGMP binding to the wild-type and mutant HCN2 C-terminus.

Results

A model for cAMP facilitation of HCN2 channel opening

cAMP facilitates the opening of the HCN2 channel by shifting the current activation curve, which is the range of voltages over which the channel opens, to less negative potentials. We have developed a nonequilibrium steady-state model for the effect of cAMP on the channel that is focused on this depolarizing shift of the current activation curve, which occurs with little change in the slope of this relationship (see Materials and methods). We assumed that each HCN2 channel is made up of four identical

subunits, each containing a single binding site, and initially, we focused on experiments from a previous study that used HCN2 channels with a varying number of functional binding sites (Ulens and Siegelbaum, 2003). In those experiments, voltage-clamp measurements of channel activity were made in membrane patches excised from *Xenopus* oocytes that expressed mouse HCN2 channels, in which the CNBDs were sequentially rendered nonfunctional by replacing arginine 591 with glutamate (R591E).

We began with a model of cAMP binding and facilitation of opening to simulate the simplest condition, which is an HCN2 channel with one functional cAMP binding site (Fig. 1 A). Each channel can exist in an open or closed state, and hyperpolarization of the membrane potential changes the balance between the open and the closed states. Under voltage-clamp conditions, cAMP-induced increase in channel opening results from an increased rate of channel opening or a decreased rate of channel closing or a combination of both. We used the values of cAMP binding to the tetrameric region of the HCN2 C-terminus (Chow et al., 2012; see Materials and methods), which were determined again here by ITC and demonstrated negative cooperativity (Fig. 1, B and C; and Table 1). In Fig. 1 D, the model is used to fit concentration–response data from HCN2 channels containing one, two, three, and four functional wild-type cAMP binding sites, which was obtained in a previous study (Ulens and Siegelbaum, 2003). We assumed that the binding values determined by ITC approximate those that occur under steady-state measurements of channel activity in the excised patch experiments.

The fit of the model to the experimentally obtained data for a channel with one fully functional binding site uses the high-affinity binding value only (for both the closed and open channel) and results from an adjustment of the transitions between the closed and open channels with one cAMP bound (Table 2). Thus, in this model, the binding affinity is not altered by pore opening. There is experimental evidence that HCN pore opening may impact cAMP binding, using fluorescent cAMP analogues (Kusch et al., 2010; Idikuda et al., 2019), but because we measured binding in the absence of the pore, we chose to make no assumptions as to whether our binding values might reflect those for open or closed channels. A future goal will be to determine how voltage-dependent channel opening, and potential associated changes in cAMP binding, might impact the concentration–response relation for the HCN2 channel using our model as a starting point. The model predicts that the maximum shift in the activation voltage at saturating levels of cAMP is a direct measure of the ratio between the opening and closing rate constants. These parameters remain unchanged when fitting the model to data obtained with additional functional binding sites. Each time one additional functional binding site is added, parameters to previously considered binding are all fixed (see below).

In the mathematical model, the value for q (the slope factor from the Boltzmann equation) was set at 5 mV, which was based on values published previously by the Siegelbaum group for cAMP effects in patches excised from *Xenopus* oocytes that expressed the HCN2 channel, e.g., Chen et al. (2001). This slope factor is a determinant of the maximum shift produced by cAMP or cGMP in our model (see Materials and methods). We assumed that this value of q was unchanged by cGMP or by mutations that did not change the maximum response to cAMP and cGMP.

The same approach was followed for two, three, and finally four fully functional binding sites, using the high-affinity binding value for the first bound cAMP molecule and the low-affinity binding values for the three cAMP molecules that bind subsequently. Thus, the model assumes that there are no further interactions between binding sites after the first site is occupied. This comes from the stoichiometry of binding of cAMP, which as determined by ITC suggested that one subunit is bound with high affinity and three subunits are bound with low affinity (Chow et al., 2012). In each case, the parameters, already determined for the closed-to-open transition of the liganded channel by fitting the experimental data with one less binding site, were assumed to not change upon the addition of subsequent binding sites; e.g., the opening and closing parameters determined from fitting the experimental data for a channel with one active binding site were fixed when fitting the experimental data for a channel with two active binding sites, and so on. With each additional functional binding site, the maximum shift in activation voltage at saturating levels is a direct measure of the ratio between rate constants, with the corresponding number of cAMPs bound to the channel. The final fits of the individual data points obtained previously by experiment (Zhou and Siegelbaum, 2007) is generally good, except for one data point at low cAMP concentration for a channel with four functional binding sites. These results predict that binding of cAMP to each additional functional site further shifts the balance toward increased opening-to-closing ratio, as reflected by the increase in the maximum voltage shift at saturating levels of cAMP with each addition of one more functional binding site. To test the validity of the model, we proceeded with analyzing several mutations within the cAMP binding site (Fig. 1 D).

A conserved arginine and threonine residue in the phosphate-binding region controls cAMP binding affinity

We used the model to help understand how key regions and residues of the cyclic nucleotide binding site impact the sensitivity of HCN2 channel opening to cAMP. To do this, we used the above model and previous data on cAMP facilitation of HCN2 channel opening in the wild-type channel and in mutants containing single alanine substitutions in the binding site (Zhou and Siegelbaum, 2007), together with measurements of cAMP binding affinity by ITC on the HCN2 C-terminal wild-type protein or proteins with corresponding substitutions. We modeled the concentration–response curves for the wild-type HCN2 mutant channels from a previous study (Zhou and Siegelbaum, 2007), which showed that some single-point alanine substitutions in the ligand binding region produced mild to moderate changes in the potency of cAMP, but did not alter the maximum effect of cAMP or gating of the channel in the absence of ligand.

We first focused on a region within the β-roll of the CNBD that binds to the phosphate group of cAMP (Fig. 2 B) and thus is referred to as the phosphate-binding cassette (PBC) in related

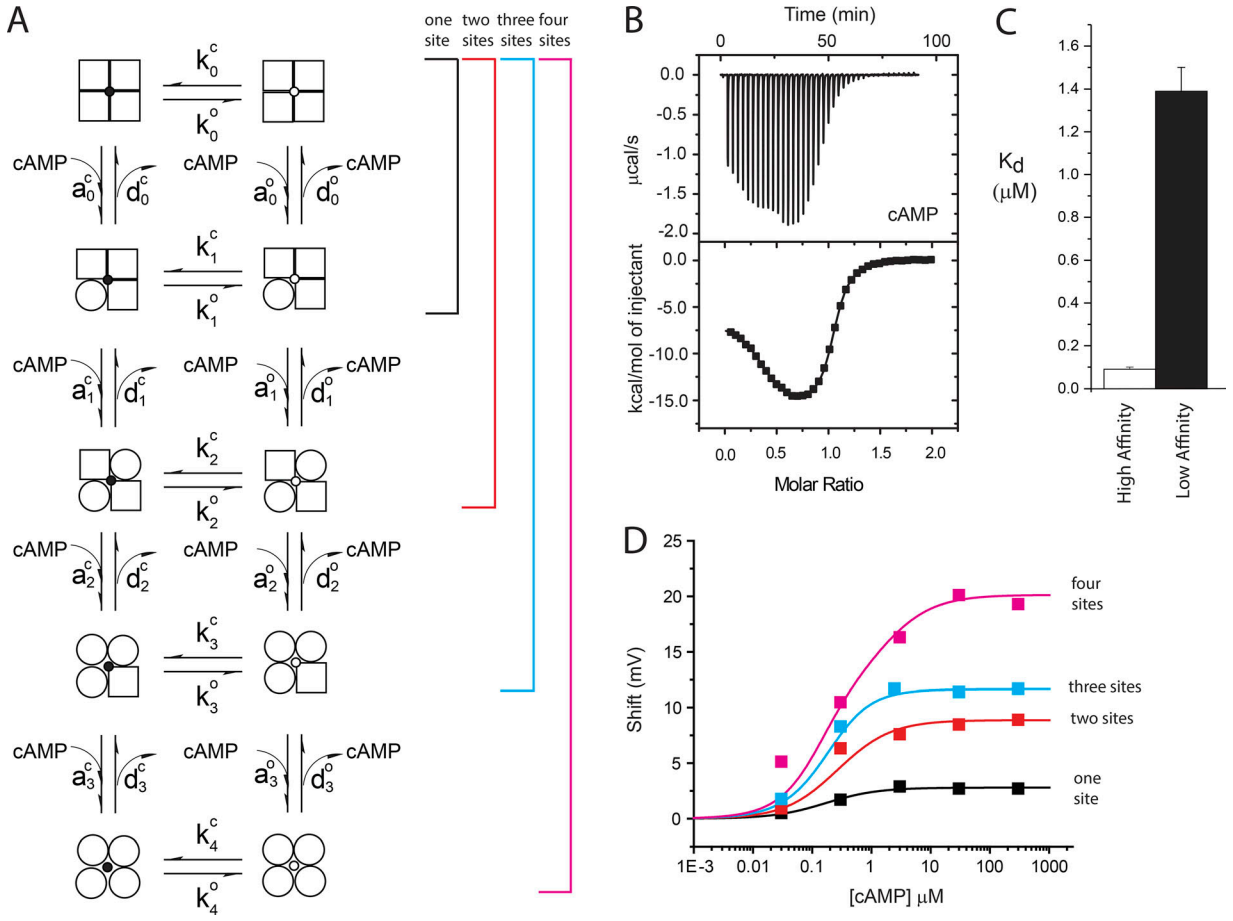

Figure 1. **A mathematical model using experimentally derived binding information describes the concentration–response curve for the effect of cAMP on the HCN2 channel with varying numbers of functional cAMP binding sites. (A)** A diagram of the model used for the facilitation of channel opening by cAMP binding to the HCN2 channel. The colored parentheses on the right show the part of the model used to simulate the concentration–response curves for one, two, three, and four cAMP binding sites, which are shown in D. **(B)** Plots of heat produced upon progressive injections of cAMP to 200 µM of the wild-type HCN2 C-terminus, measured by ITC. The inflections in the top plot arise from injections of cAMP, where each inverted peak shows the heat difference between the sample and reference compartment. The peaks decrease in magnitude as binding sites become saturated. The lower plot shows values determined by integration of the area under the peaks from the upper plot versus the ratio of injected ligand to protein. The solid line through the values represents a two-site independent binding site model, which yielded values for affinity and energetics (ΔG, ΔH, and ΔS). **(C)** Bar graphs of high- and low-affinity binding values that arise from the fitting of the heat values with a two-site independent binding model for the binding of cAMP to the wild-type HCN2 C-terminus. Values represent means ± SEM. Each mean was determined from independent ITC binding experiments. Values for binding affinity are also given in Table 1. **(D)** Concentration–response data and simulated curves for the shift in gating produced by cAMP. The data points represent data from for the shifts produced by cAMP on a channel with one functional binding site (black squares), two functional binding sites (red squares), three binding sites (blue squares), and four binding sites (purple squares). Tetrameric HCN2 channels with one and three functional sites were formed by tandem tetramers, whereas channels with two and four binding sites were formed with tandem dimers; a highly conserved arginine residue in the PBC in the CNBD was substituted with glutamate residue to prevent binding. The data points shown are reproduced from Ulens and Siegelbaum (2003). The solid lines are theoretical curves produced by the mathematical model for channels containing the corresponding number of binding sites (shown in A).

proteins (Das et al., 2007). Arginine 591, which is found deep within the PBC, makes contact with the equatorial oxygen of the cyclic phosphate group of cAMP and cGMP (Zagotta et al., 2003; Zhou and Siegelbaum, 2007); this residue is highly conserved not only among the HCN isoforms (Jackson et al., 2007), but also in many proteins containing this family of CNBDs (Weber and Steitz, 1987; Shabb and Corbin, 1992; Tibbs et al., 1998). Threonine 592, adjacent to R591, is conserved in many of the proteins in this family (Shabb and Corbin, 1992; Jackson et al., 2007) and makes contact with the axial oxygen of the cyclic phosphate group of cAMP and cGMP (Zagotta et al., 2003; Zhou and Siegelbaum, 2007). When either of these two residues was substituted with alanine, the opening and closing of the HCN2 channels in the absence of cAMP and the maximum effect of cAMP were not impacted; however, its potency was reduced (Zhou and Siegelbaum, 2007). A question that arises from those data are whether a change in binding affinity alone is sufficient to explain the reduction in potency.

Here, R591 and T592 were individually substituted by alanine in our HCN2 C-terminal protein, and binding of cAMP was analyzed by ITC. Like its binding to the wild-type protein, cAMP binding to the mutant proteins produced two-phase patterns that were best fitted with a two-site independent binding model and demonstrated negative cooperativity (Fig. 2, B and C; and

Table 1. **Dissociation constants arising from the binding of cAMP or cGMP to wild-type and mutant HCN2 C-termini**

Construct/ligand	K_d		K_d		
	μM	n	μM	n	N
cAMP					
Wild type	0.09 ± 0.01	0.33 ± 0.02	1.39 ± 0.11	0.66 ± 0.09	3
R591A	1.65 ± 0.57	0.35 ± 0.02	33.35 ± 5.58	0.70 ± 0.09	3
T592A	0.61 ± 0.25	0.23 ± 0.01	11.83 ± 4.37	0.56 ± 0.06	3
I630A	0.19 ± 0.06	0.28± 0.03	3.10 ± 0.74	0.69 ± 0.07	4
D631A	0.11 ± 0.01	0.21 ± 0.02	1.90 ± 0.27	0.56 ± 0.04	3
L633A	1.32 ± 0.27	0.41 ± 0.02	23.19 ± 3.29	0.69 ± 0.05	5
D634A	0.10 ± 0.03	0.26 ± 0.03	1.39 ± 0.46	0.81 ± 0.03	5
R635A[a]	0.19 ± 0.04	0.35 ± 0.02	2.19 ± 0.40	0.45 ± 0.02	4
I636A	0.47 ± 0.04	0.36 ± 0.01	6.94 ± 0.31	0.60 ± 0.03	4
I636D	0.74 ± 0.29	0.56 ± 0.07	17.16 ± 2.34	0.82 ± 0.02	3
K638A	0.31 ± 0.15	0.38 ± 0.04	8.00 ± 2.48	0.50 ± 0.03	4
cGMP					
Wild type	0.36 ± 0.05	0.21 ± 0.01	6.13 ± 0.22	0.27 ± 0.01	2
R591A	321.71 ± 26.72	2.15E-5 ± 9.20E-6			2
T592A	183.53 ± 2.69	0.20 ± 0.03			2
I630A	0.49 ± 0.11	0.24 ± 0.05	7.78 ± 0.31	0.44 ± 0.05	4
D631A	0.21 ± 0.06	0.20 ± 0.03	4.78 ± 0.88	0.63 ± 0.09	5
L633A	16.52 ± 3.20	0.74 ± 0.09			5
D634A	0.54 ± 0.10	0.23 ± 0.04	8.04 ± 1.32	0.87 ± 0.14	5
R635A[a]	4.61 ± 0.16	0.67 ± 0.09			4
I636A	0.24 ± 0.02	0.23 ± 0.01	3.23 ± 0.15	0.44 ± 0.02	4
I636D	0.21 ± 0.07	0.18 ± 0.04	1.76 ± 0.51	0.56 ± 0.08	4
K638A	14.69 ± 2.04	0.47 ± 0.09			3

The table summarizes the dissociation constants (K_d) in micromoles per liter, which were determined from fitting of heat released upon binding by one or two independent site binding models as indicated. Values represent means ± SEM.
[a]For R635A, the value represents the mean of four trials, three of which were taken from our previous publication (Ng et al., 2016) and another which was carried out for this study.

Table 1). The thermodynamic profile of cAMP binding to the R591A and T592A mutant proteins is similar to that of the wild-type protein, in that the high-affinity binding possesses favorable changes in both enthalpy and entropy, whereas low-affinity binding is associated with favorable changes in enthalpy but unfavorable changes in entropy. Even though the change in enthalpy for high-affinity binding is smaller than that for low-affinity binding, the favorable change in entropy for the former results in the more favorable change in free energy. By contrast, low-affinity binding is associated with unfavorable change in entropy. Thus, the thermodynamic basis for negatively cooperative binding of cAMP is mainly entropic for these mutants, as well as for the wild-type protein.

We then used the mathematical model to find out if it would predict the experimental concentration–response data for the R591A and T592A mutant channels. With small adjustments, the wild-type concentration–response data from Zhou and Siegelbaum (2007) were well fitted by the model using experimental binding affinities determined here by ITC (Fig. 2 D). We then incorporated the binding affinities of the mutants into the model without altering the wild type closed-to-open parameters. Remarkably, the theoretical curves overlie closely to the experimentally determined concentration–response data for the corresponding full-length mutant HCN2 channels; both are shifted to the right compared with the curve and data obtained for cAMP binding to the wild-type channel (Fig. 2 D). Thus, the shift in the concentration–response data produced experimentally by the R591A and T592A mutations can be accounted for entirely by reduced binding affinities (as measured by ITC) without any impact on the transitions between pore opening and closing.

Residues in the distal C-helix of the CNBD contribute to both cAMP binding affinity and effects on gating

We next examined residues in the C-helix region, which is at the distal end of the CNBD. The importance of this region is

Table 2. **Parameters of the mathematical model used to simulate concentration–response data**

Parameter	cAMP	cGMP			cAMP						
		Wild type	I636A	I636D	Wild type	R591A	T592A	R635A	I636A	I636D	K638A
q (mV)	5	5	5.76	6.72	5	5	5	5.1	5.36	5.05	5
K_d (μM)											
Site 1	0.15	0.36	0.24	0.21	0.09	1.64	0.61	0.2	0.47	0.74	0.31
Site 2	1.5	6.13	3.23	1.76	1.39	33.35	11.83	2.19	6.94	17.16	8.00
Site 3	1.5	6.13	3.23	1.76	1.39	33.35	11.83	2.19	6.94	17.16	8.00
Site 4	1.5	6.13	3.23	1.76	1.39	33.35	11.83	2.19	6.94	17.16	8.00
k_1^c	0.75	0.7	0.1	0.06	1.6	1.6	1.6	0.8	1	0.15	1.6
K_1	1.76	1.6	2.3	2.4	1.01	1.01	1.01	1.1	1.5	1.4	1.01
k_{j2}^c	9.6	4	0.02	0.08	10	10	10	7	4	0.1	10
K_2	5.36	12	2.8	9	4	4	4	3	4	10	4
k_3^c	43	100	0.02	0.05	80	80	80	40	4	0.1	80
K_3	10.85	14	4	18	38	38	38	8	38	12	38
k_4^c	120	120	0.062	0.05	120	120	120	110	4	0.02	120
K_4	59	33.5	33	33	40	40	40	40	40	40	40

The table summarizes the sets of parameters of the mathematical model used for three sets of data for concentration versus the depolarizing shift in the activation curve. cAMP parameters are used to simulate the concentration–response data from Ulens and Siegelbaum (2003), which were used to set up the initial model and are shown in Fig. 1 A along with the simulated curves. cGMP parameters are used to simulate the concentration–response data from Zhou and Siegelbaum (2007). Note that curves for wild-type channel and cGMP were also produced using the gating parameters (k_j^c and K_j) for wild type and cAMP. Also, curves for I636A and I636D, with cGMP, were produced using the gating parameters (k_j^c and K_j) for the wild-type channel and cGMP. cAMP parameters were used to simulate the concentration–response data from Zhou and Siegelbaum (2007). Note that curves for R635A, I636A, and I636D were also produced using the gating parameters (k_j^c and K_j) for the wild-type channel and cAMP.

highlighted by studies showing that partial truncations of the HCN2 C-terminus, which include the C-helix, or alanine substitution of arginine 632 in this helix, eliminate the cAMP-induced shift in channel activation (Wainger et al., 2001; Zhou and Siegelbaum, 2007). Furthermore, there is considerable functional and structural evidence in both HCN and CNG channels that, upon ligand binding, the C-helix moves relative to the ligand (Goulding et al., 1994; Varnum et al., 1995; Matulef et al., 1999; Matulef and Zagotta, 2002; Mazzolini et al., 2002; Puljung and Zagotta, 2013) and toward the phosphate-binding region within the β-roll (including R591 and T592 in HCN2), which is thought to move very little relative to the ligand and transmembrane regions (Tibbs et al., 1998; Flynn et al., 2007; Zhou and Siegelbaum, 2007; Taraska et al., 2009; Akimoto et al., 2014; Puljung et al., 2014; Saponaro et al., 2014; DeBerg et al., 2016; Lee and MacKinnon, 2017). Finally, in the absence of cAMP, the C-terminal portion of the C-helix is less structured in HCN1, HCN2, and HCN4 (Taraska et al., 2009; Puljung and Zagotta, 2013; Akimoto et al., 2014; Puljung et al., 2014; Saponaro et al., 2014; Lee and MacKinnon, 2017).

We first focused on residues in the distal C-helix, R635, K638, and I636, which are found near to the adenine portion of cAMP based on x-ray crystallography (Fig. 3 A), functional analysis of mutant proteins (Zagotta et al., 2003; Flynn et al., 2007), and molecular dynamics simulations of the C-linker and CNBD (Zhou and Siegelbaum, 2007). When these residues were individually substituted with alanine, the opening and closing of the HCN2 channels in the absence of cAMP were not affected and the maximum effect of cAMP was not affected but its potency was reduced (Zhou and Siegelbaum, 2007). Here, too, we wondered if a change in binding affinity alone is sufficient to explain the reduction in potency.

These three residues were individually substituted with alanine in the HCN2 C-terminal protein, and the binding of cAMP was examined by ITC, which resulted in a two-phase pattern that was best fitted with a two-site independent binding model and demonstrated negative cooperativity (Fig. 3 B). The thermodynamic profiles of cAMP binding to the three mutated fragments were, again, similar to that in the wild-type protein (Fig. 3 C). The values for K_d were variably increased by the three alanine substitutions; for R635A, which points away from the ligand in the crystal structure, the reduction was smallest, whereas it was larger for I636A and K638A, which point toward the ligand in the crystal structure.

The values for binding affinity were substituted into the model without altering the values of closed-to-open transitions determined for the wild-type channel, and these theoretical curves were overlaid onto the previously determined concentration–response data (Fig. 3 D). Notably, the theoretical curve for R635A is shifted little, whereas that for I636A is shifted to the right to a greater extent compared with the wild type concentration–response data; neither is as right-shifted as the experimental concentration–response data for the corresponding mutant channel. To fit the concentration–response data, further changes

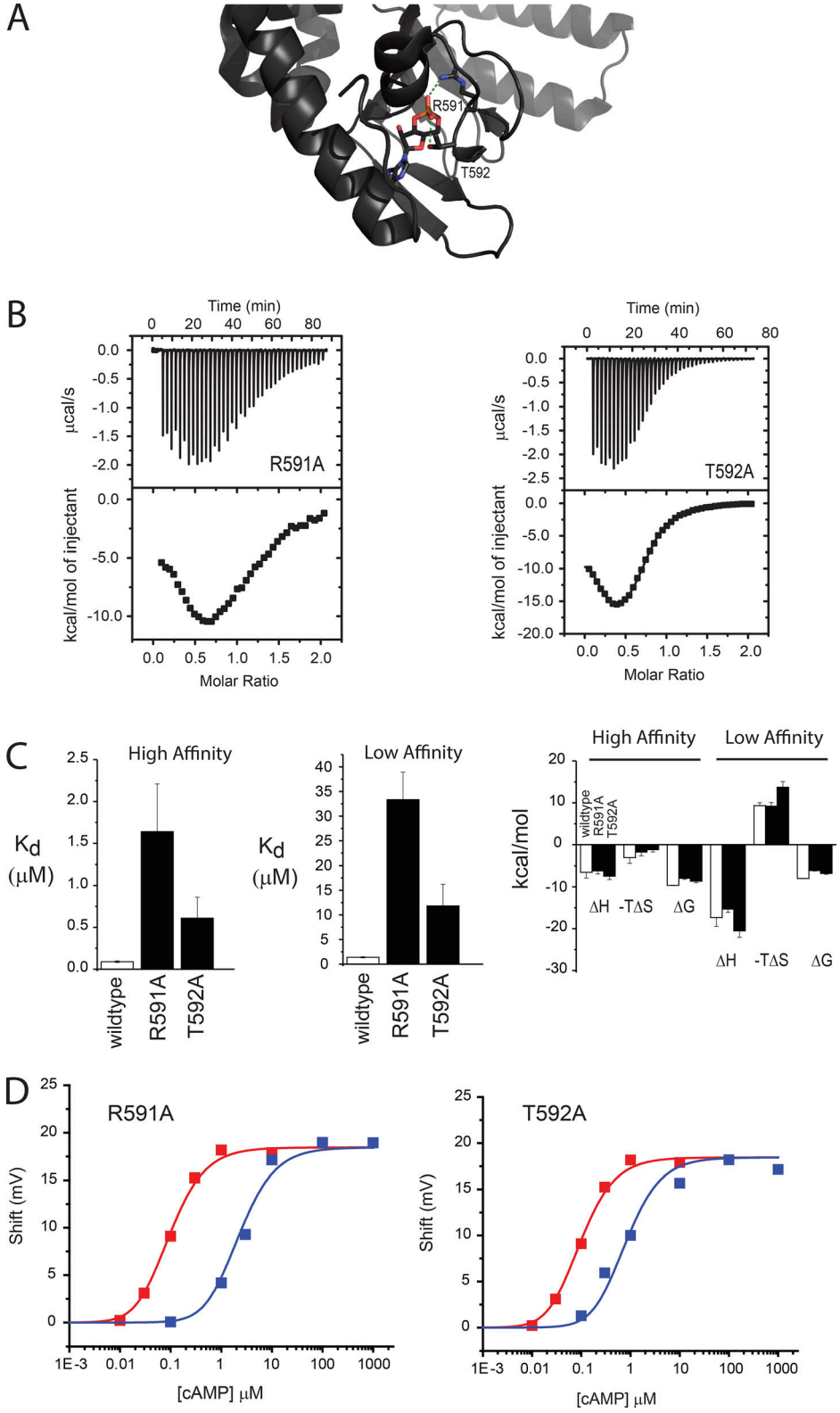

Figure 2. **Two conserved residues of PBC contribute to cAMP binding affinity but do not alter channel opening. (A)** A ribbon diagram showing the position of R591 and T592, which are deep in the phosphate binding region of the CNBD and were individually substituted with alanine. PDB accession no. 1Q50. Their side chains form hydrogen bonds with the phosphate oxygen, shown in green. **(B)** Plots of heat produced upon progressive injections of cAMP to 200 µM of R591A and T592A HCN2 C-terminus, measured by ITC. The inflections in the top plot arise from injections of cAMP, where each inverted peak shows the heat difference between the sample and reference compartment. The peaks decrease in magnitude as binding sites become saturated. The lower plot shows values determined by integration of the area under the peaks from the upper plot versus the ratio of injected ligand to protein. The solid line through the values represents a two-site independent binding site model, which yielded values for affinity and energetics (ΔG, ΔH, and ΔS). **(C)** Bar graphs of high-affinity

(left) and low-affinity (middle) binding values and thermodynamics (right) that arise from the fitting of the heat values with a two-site independent binding model for the binding of cAMP to the two mutant C-termini (as in B) and the wild-type HCN2 C-terminus. Values represent means ± SEM. Each mean was determined from independent ITC binding experiments. Values for binding affinity and stoichiometry are also given in Table 1. **(D)** Concentration–response data and theoretical curves for the shift in activation gating produced by cAMP. The solid red lines are produced by the mathematical model using the experimental binding affinities obtained by ITC for the wild-type protein and fitted to the concentration–response data for the wild-type channel (red squares). The solid blue lines are produced by the mathematical model using the experimental binding affinities obtained for cAMP binding to the mutant proteins but using the gating parameters that were obtained from the fit of the model to the wild-type data. Note how well the theoretical blue curves fit the experimental concentration–response data for the mutant channels (blue squares). The concentration–response data were reproduced from Zhou and Siegelbaum (2007).

in the closed-to-open transitions were necessary, more so for R635A than I636A (Table 2). Thus, both residues may contribute directly to the opening of the liganded channel. The theoretical curve for K638A is also shifted to the right of the wild type concentration–response data but, in contrast to the theoretical curves for the R635A and I636A channels, it fits the concentration–response data for the full-length version of the K638A channel very well. This suggests that the effect of the K638A substitution on the concentration–response data can be accounted for entirely by reduced binding affinities, without any impact on the opening and closing transitions of the pore.

The role of other C-helix residues in cAMP binding

We also examined the role of five other residues in the distal C-helix (Fig. 4 A) in cAMP binding, for which a full range of concentration–response data were not available. By ITC, we found that cAMP binding to I630A, D631A, L633A, and D634A proteins produced heat values that fitted well with a two-site independent binding model (Fig. 4 B). The thermodynamics of binding of cAMP to these four mutant fragments were again, in general, similar to those obtained by cAMP binding to the wild-type protein (Fig. 4 C). For I630A, D631A, and D634A, the K_d values were not greatly altered (Fig. 4 D and Table 1), which is consistent with their small effects on potency (Zhou and Siegelbaum, 2007). As can be seen in the structure (Fig. 4 A), these three residues are also facing away from cAMP, which might support the small effect on binding and potency. The L633A mutation reduced cAMP binding affinity to a larger extent than the other alanine substitutions (Fig. 4 D and Table 1), which is consistent with the larger reduction in cAMP potency found previously (Zhou and Siegelbaum, 2007). Also, unlike the other three residues, L633 is pointing toward the ligand, which supports a more direct role in binding for this residue (Fig. 4 A).

Arginine 632 is of interest because alanine substitution of this residue eliminates the shift of the channel activation curve to more negative voltages; this is the only mutation analyzed in the current article that strongly reduces the maximum shift produced by cAMP or cGMP (Zhou and Siegelbaum, 2007). Arginine 632 makes a very strong electrostatic interaction with the adenine portion of cAMP as well as a salt bridge with glutamate 582, which interacts with the 2′OH in the ribose moiety of cAMP (Zagotta et al., 2003; Zhou and Siegelbaum, 2007). Glutamate 582 is found in the P-helix, a region between the sixth and seventh β-sheets, and becomes structured and interacts with the B-helix upon cAMP binding (Taraska et al., 2009; Saponaro et al., 2014). Unlike alanine substitution of R632, alanine substitution of E582 allows cAMP to shift the voltage dependence of channel opening by the same maximum amount as the wild-type channel, but its potency is reduced much more than the other alanine mutants (Zhou and Siegelbaum, 2007), which suggests that this salt bridge between the C- and P-helices is important for the latter but not for the former.

To understand how R632 and E582 influence binding, we purified the mutated C-linker/CNBD with HMT tag (see Materials and methods) on its N-terminus; these proteins could not be purified in high enough amounts to assess binding after cleaving the HMT tag. We found previously that HMT-fused C-terminus and untagged C-terminus wild-type proteins bind cAMP in a similar fashion, as determined by ITC (with negative cooperativity), which suggests that HMT does not interfere with the binding site, protein folding, or oligomerization (Chow et al., 2012). Here, we found that cAMP binding to the E582A-HMT protein produced a pattern of heat release that was best fitted with a single independent binding site model and yielded an average K_d of 335 µM for two trials (Fig. S1). The lack of negative cooperativity could mean that negative cooperativity is no longer observed because either cooperativity is abolished or the residual effect is too small to be resolved. Finally, in two trials, binding of cAMP to R632A-HMT protein was not detected (not depicted).

We also used another cAMP analogue to examine the interactions of E582 and R632 with the 2′OH group of cAMP. The interaction could potentially be disrupted by capping the 2′-hydroxyl group of cAMP with a methyl group (2′-O-Me-cAMP), which has been shown to bind to the Epac cAMP-binding protein (Christensen et al., 2003), but not to a monomeric form of HCN2 C-terminus (Möller et al., 2014). Because we have previously shown that a monomeric form of the HCN2 fragment possesses only the low-affinity cAMP-binding site (Chow et al., 2012), we examined the binding of this analogue to the tetrameric form of the HCN2 C-linker/CNBD, which also possesses the high-affinity binding site. However, in two trials, we found that 2′-O-Me-cAMP did not bind to the tetrameric form of the HCN2 C-terminus (not depicted). Together, the data suggest that the internal salt bridge and interactions of these residues with the ligand are necessary for keeping the C-linker/CNBD structure stable and for maintaining high affinity for the ligand.

The difference in sensitivity of HCN2 channel opening to cAMP and cGMP is due to a difference in binding affinity and allosteric effects on gating

We next examined the difference in potency of cAMP and cGMP on the HCN2 channel. Although both molecules produce a similar maximum effect, cAMP is a more potent facilitator of HCN2 channel opening than cGMP (Zagotta et al., 2003; Zhou and

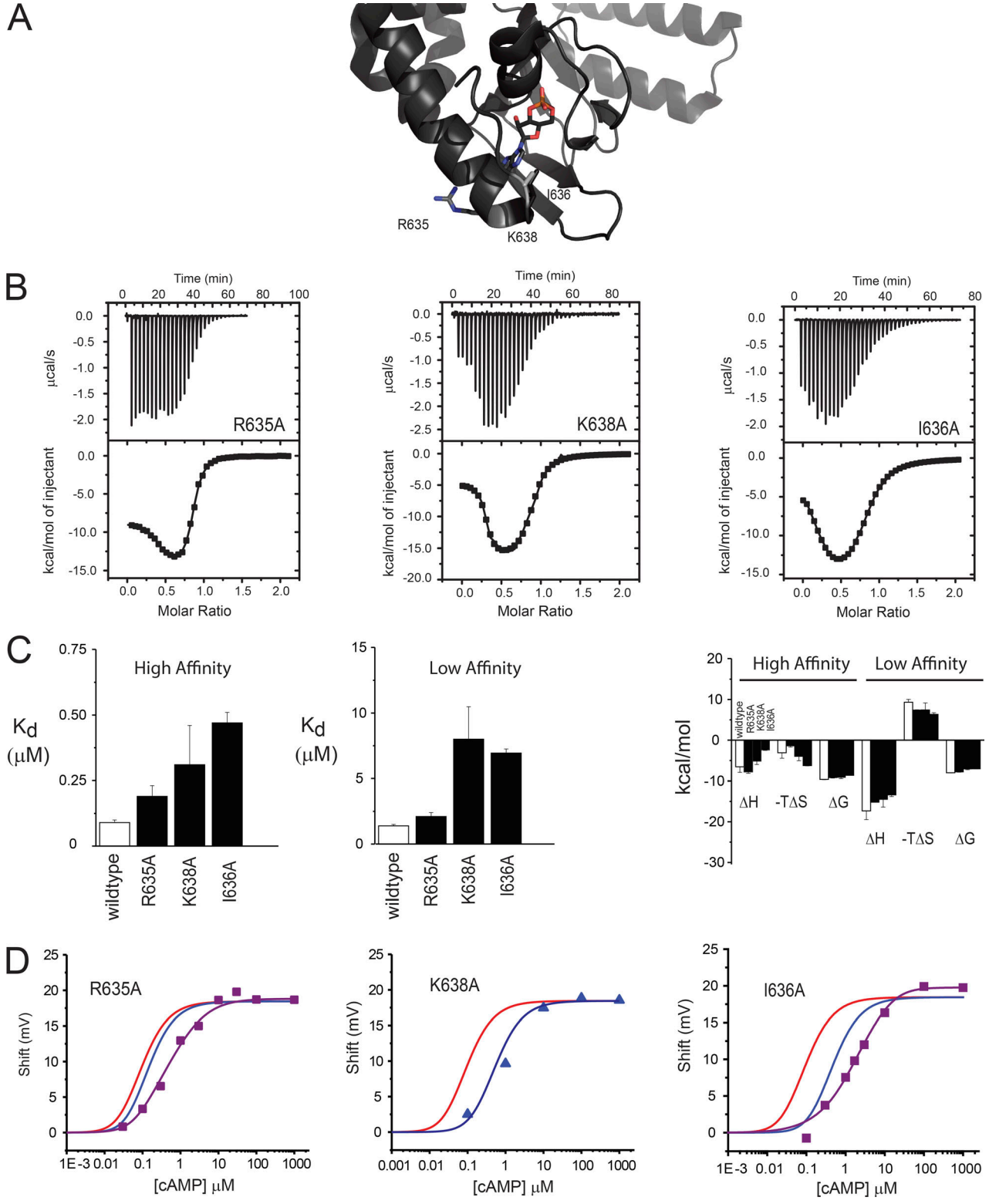

Figure 3. **Residues of the C-helix contribute to ligand binding affinity and variably couple binding to channel opening. (A)** A ribbon diagram showing the position of R635, I636, and K638, which are located in the C-helix at the distal region of the CNBD. PDB accession no. 1Q50. **(B)** Plots of heat produced upon progressive injections of cAMP to 200 µM of R635A, I636A, and K638A HCN2 C-terminus, measured by ITC. The inflections in the top plot arise from injections of cAMP, where each inverted peak shows the heat difference between the sample and reference compartment. The peaks decrease in magnitude as binding sites become saturated. The lower plot shows values determined by integration of the area under the peaks from the upper plot versus the ratio of injected ligand to protein. The solid line through the values represents a two-site independent binding site model, which yielded values for affinity and energetics (ΔG, ΔH, and ΔS). Values for binding affinity are shown in Table 1. **(C)** Bar graphs of high-affinity (left) and low-affinity (middle) binding values and thermodynamics (right) that arise from the fitting of the heat values with a two-site independent binding model for the binding of cAMP to the mutants (as in

B) and the wild-type HCN2 C-terminus. Values represent means ± SEM. Each mean was determined from independent ITC binding experiments. Values for binding affinity are also given in Table 1. **(D)** Concentration–response data and theoretical curves for the shift in activation gating produced by cAMP. The solid red lines are produced by the mathematical model using the experimental binding affinities obtained by ITC for the wild-type protein and fitted to the concentration–response data for the wild-type channel. The solid blue lines are produced by the mathematical model using the experimental binding affinities obtained for cAMP binding to the corresponding mutant proteins but using the gating parameters that were obtained from the fit of the model to the wild-type data. Note that the blue line for the K638A channel fits the concentration–response data (blue squares) very well (middle graph). However, the blue lines for the R635A and I636A channels do not fit the concentration–response data (purple squares) very well; the open and closing transitions were therefore also changed to produce theoretical curves (purple lines) that fit the concentration–response data for those mutants appropriately. The concentration–response data were reproduced from Zhou and Siegelbaum (2007).

Siegelbaum, 2007). In part, this may be due a difference in configuration between them upon binding; in the crystal structure, cAMP and cGMP were shown to bind in the *anti* and *syn* configuration, respectively (Fig. 5 A). We again performed ITC to determine if the difference in potency between cAMP and cGMP is primarily due to a difference in the binding affinity to the CNBD. As we found previously (Ng et al., 2016), cGMP, like cAMP, produced a two-phase pattern in the binding isotherm that could be best fitted with a two-independent binding site model (Fig. 5 B); this yielded high- and low-affinity binding values of ∼0.36 and 6.13 µM, respectively (Fig. 5 C and Table 1). The values of binding affinity for cGMP are lower than those for cAMP, which were 0.09 and 1.39 µM. Thus, for cGMP binding, the high-affinity K_d is increased by threefold, whereas the low-affinity K_d is increased by ∼3.4-fold, compared with cAMP binding, which suggests that cAMP may produce a greater degree of negative cooperativity than cGMP. The thermodynamics of cGMP binding the HCN2 C-terminal fragment are similar to those obtained for cAMP (Fig. 5 D); negative cooperativity was driven by changes in entropy.

We used the model to determine how the difference in binding affinity between cAMP and cGMP contributes to the difference in the measured concentration–response data. We introduced the binding affinities determined for cGMP by ITC into the model without altering the closed-to-open transitions that were determined for cAMP to generate a theoretical concentration–response curve, which is predictably shifted to the right compared with the curves for cAMP (Fig. 5 E). However, the concentration–response data for cGMP are right-shifted to a much greater extent than the theoretical cGMP curve. To fit the experimental data, alterations to the transition rates between open and closed pores were also necessary (Table 2). Thus, our analysis suggests that the greater potency of cAMP on facilitation of HCN2 channel opening compared with cGMP is due to enhanced transition rates between the closed and open pore as well as greater binding affinity.

Isoleucine 636 contributes to cAMP selectivity by enhancing cAMP binding affinity and gating, and by reducing cGMP binding affinity

Previous studies have suggested that isoleucine 636 (I636) in the C-helix of the HCN2 channel may confer some of the selectivity for cAMP over cGMP (Flynn et al., 2007; Zhou and Siegelbaum, 2007). Above (Fig. 3), we show that alanine substitution of I636 in the C-helix decreases the affinity for cAMP but that it may also decrease promotion of the closed-to-open transitions. Here, by ITC, we found that cGMP binding to the I636A mutant protein also produced a two-phase pattern in the binding isotherm that could be well fitted with a two-site independent binding model (Fig. 6 A). This alanine substitution produced a modest increase in the affinity for cGMP (Fig. 6 C and Table 1). Thus, as expected, the isoleucine side chain normally inhibits cGMP binding, in contrast to its effect on cAMP binding. The overall pattern of thermodynamics is similar to that for cGMP binding to the wild-type C-terminus (Fig. 6 D).

We next examined how the alterations in binding affinity contribute to the difference in the cGMP concentration–response curve (Fig. 6 E). The simulated I636A curve, which uses gating parameters obtained from the fit of the mathematical model to the cGMP concentration–response data of the wild-type channel, follows closely, but not exactly, the experimental data, which are shifted to the left of the wild type concentration–response data. Small adjustments in gating transitions allow the simulation to fit the experimental data. Nevertheless, these data suggest that the isoleucine promotes cAMP selectivity over cGMP mainly by reducing cGMP binding affinity, as well as by augmenting cAMP binding affinity and promotion of gating, which was suggested above in Fig. 3.

To further investigate the role of I636 in selectivity, we substituted an aspartate residue for I636 (I636D), which was shown previously to greatly enhance the potency of cGMP for HCN2 channel opening (Flynn et al., 2007; Zhou and Siegelbaum, 2007). A crystal structure of the I636D C-terminus shows that the aspartate residue forms a new contact with the guanine ring of cGMP (Fig. 6 B; Flynn et al., 2007). By ITC, cGMP binding to the I636D mutant fragment was found to produce a two-phase pattern in the released heat that was well fitted with a two-site independent binding model (Fig. 6 A). The aspartate substitution produced a large increase in the affinity for cGMP, larger than did the alanine substitution (Fig. 6 C and Table 1), which fits with the novel interaction suggested previously (Flynn et al., 2007). The thermodynamic pattern of cGMP binding was similar to that for cGMP binding to the wild-type and the I636A protein (Fig. 6 D).

We next examined how the change in cGMP binding by I636D contributes to the altered concentration–response curve (Fig. 6 E). Again, without altering the closed-to-open transitions for the wild-type channel response to cGMP, we introduced the cGMP binding affinities determined for the I636D mutant into the mathematical model. As for the I636A mutant, the simulated curve for the I636D overlies closely the experimental concentration–response data, which are shifted to the left of the wild type concentration–response data. Thus, changes in the cGMP concentration–response curve induced by the aspartate

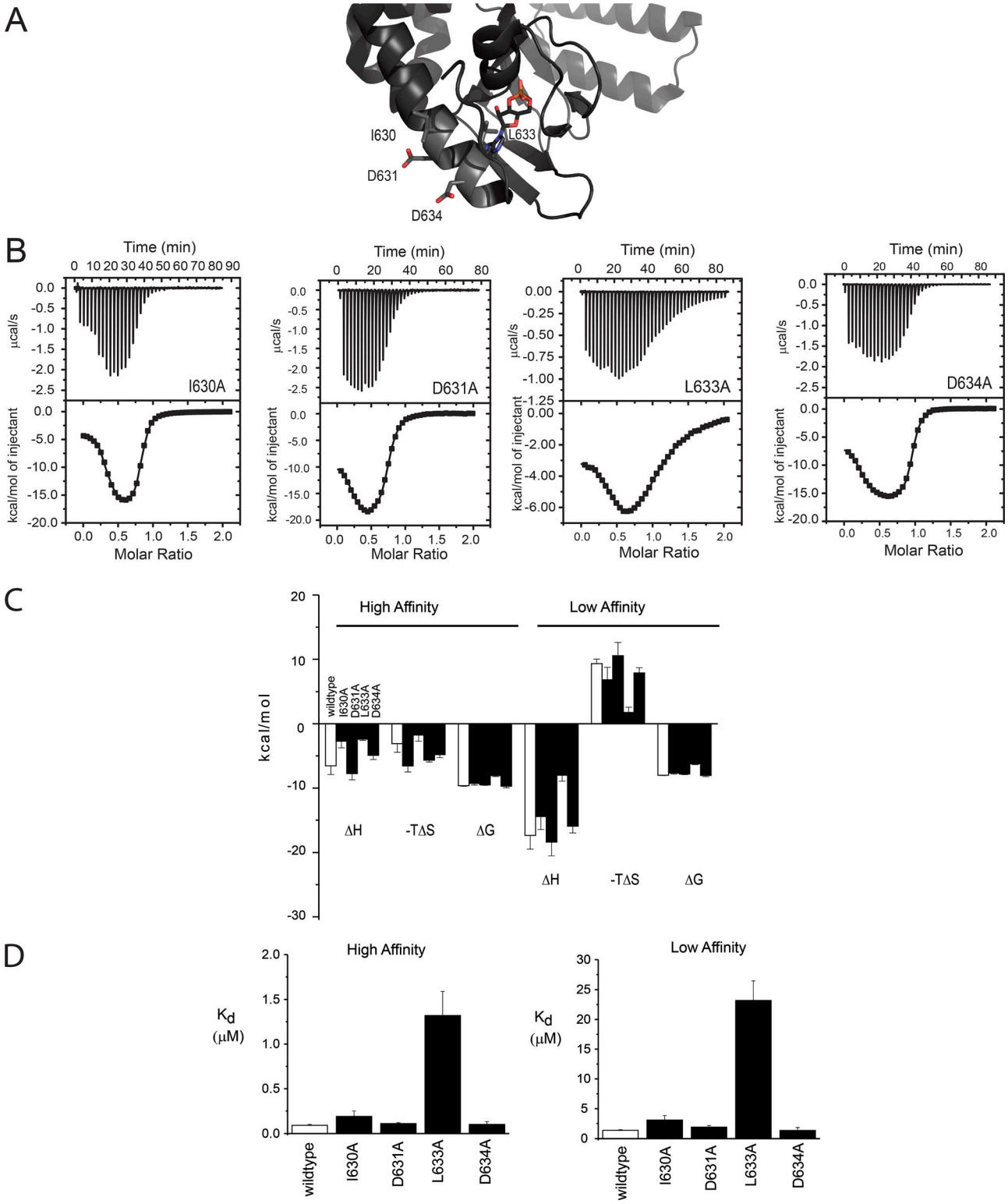

Figure 4. **Other C-helix residues make variable contributions to cAMP binding to the tetrameric HCN2 C-terminus. (A)** A ribbon diagram showing the position of I630, D631, L633, and D634, which are located in the C-helix at the distal region of the CNBD. PDB accession no. 1Q50. **(B)** Bar graphs of heat produced upon progressive injections of cAMP to 200 µM of the mutant or wild-type HCN2 C-terminus, measured by ITC. The inflections in the top plot arise from injections of cAMP, where each inverted peak shows the heat difference between the sample and reference compartment. The peaks decrease in magnitude as binding sites become saturated. The lower plot shows values determined by integration of the area under the peaks from the upper plot versus the ratio of injected ligand to protein. The solid line through the values represents a two-site independent binding site model, which yielded values for affinity and energetics (ΔG, ΔH, and ΔS). **(C)** Bar graph of thermodynamics parameters that arise from the fitting of the heat values with a two-site independent binding model for the binding of cAMP to the mutants (as in B) and the wild-type HCN2 C-terminus. **(D)** Bar graphs of binding affinities that arise from the fitting of the heat values with two-independent binding site model for the binding of cAMP to the mutants (as in B) and the wild-type HCN2 C-terminus. Values for binding affinity are shown in Table 1. Values in C and D represent means ± SEM. Each mean was determined from independent ITC binding experiments.

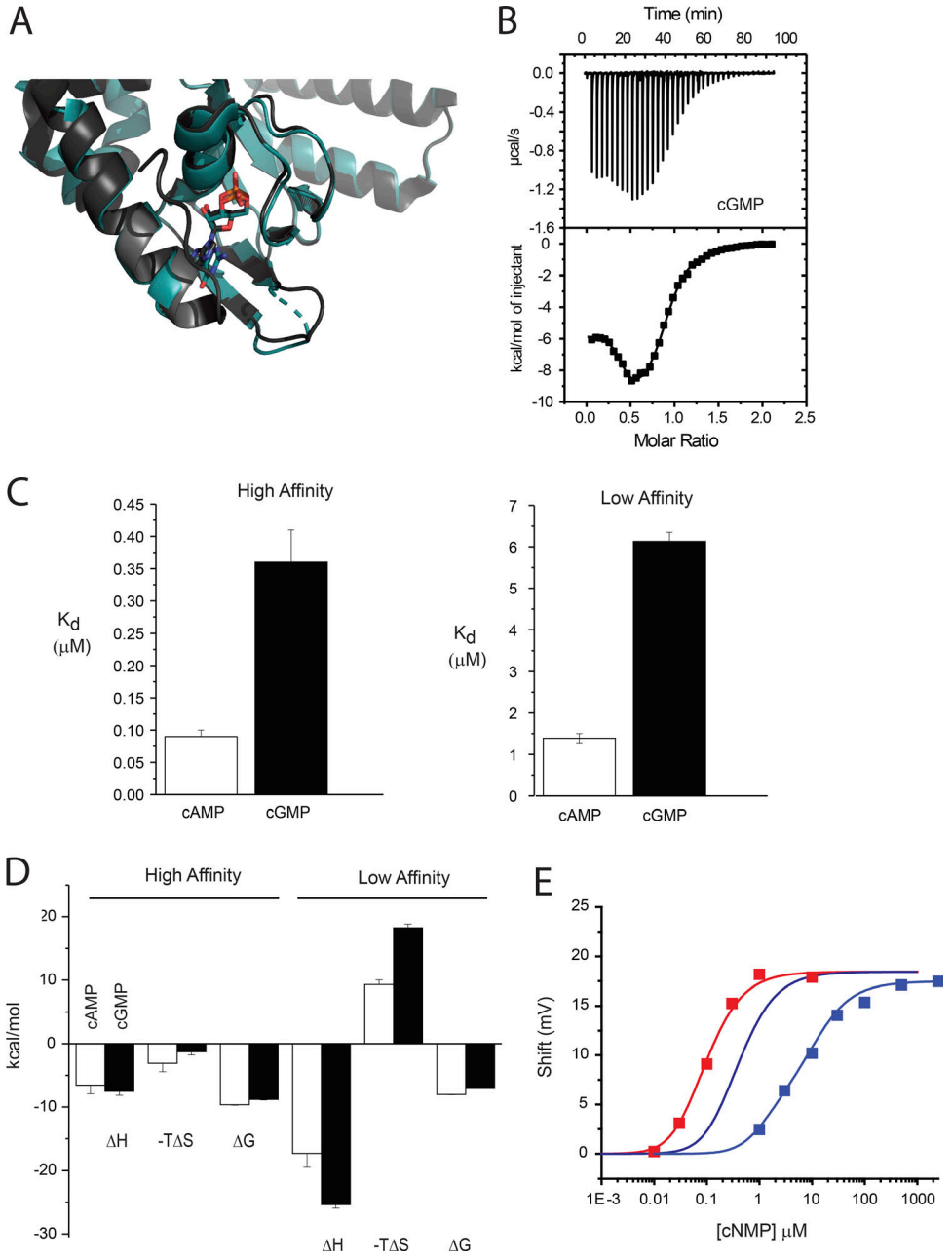

Figure 5. **The greater potency of cAMP versus cGMP is due to greater binding affinity and stronger effects on channel opening. (A)** A ribbon diagram showing an overlay of the cAMP-bound and cGMP-bound structures of the wild-type HCN2 C-terminus. Note that cAMP and cGMP are bound in *anti* and *syn* configurations, respectively. Residues distal to R635 are not resolved in the cGMP-bound wild-type structure. PDB accession no. 1Q50 (cAMP bound) and PDB accession no. 1QE3 (cGMP bound). **(B)** Plots of heat produced upon progressive injections of cGMP to 200 µM HCN2 C-terminus, measured by ITC. The inflections in the top plot arise from injections of cGMP, where each inverted peak shows the heat difference between the sample and reference compartment. The peaks decrease in magnitude as binding sites become saturated. The lower plot shows values determined by integration of the area under the peaks from the upper plot versus the ratio of injected ligand to protein. The solid line through the values represents a two-site independent binding model, which yielded values for affinity and energetics (ΔG, ΔH, and ΔS). **(C)** Bar graphs of high- and low-affinity binding values that arise from the fitting of the heat values with a two-site independent binding model for the binding of cAMP and cGMP to the wild-type HCN2 C-terminus. Values for binding affinity are given in Table 1. **(D)** Bar graphs of values for thermodynamics that arise from the fitting of the heat values with a two-site independent binding model for the binding of cAMP and cGMP to the wild-type HCN2 C-terminus. Values in C and D represent means ± SEM. Each mean was determined from independent ITC binding experiments. **(E)** Concentration–response data and simulated curves for the shift in gating produced by cAMP and cGMP. The solid red line is produced by the mathematical model using the experimental binding affinities for cAMP obtained by ITC for the wild-type protein and fitted to the concentration–response data for cAMP facilitation of the wild-type HCN2 channel. The solid blue line is produced by the mathematical model using the experimental binding affinities obtained for cGMP binding to wild-type protein by ITC but using the gating parameters that were obtained from the fit of the model to the cAMP concentration–response data. Note that this blue line does not fit the cGMP concentration–response data (purple squares) for the wild-type HCN2 channel. For the model to fit the cGMP concentration–response data (purple line), changes in the transitions between the closed and open pore were necessary in addition to using the binding affinities obtained by ITC from cGMP binding to the C-terminus protein.

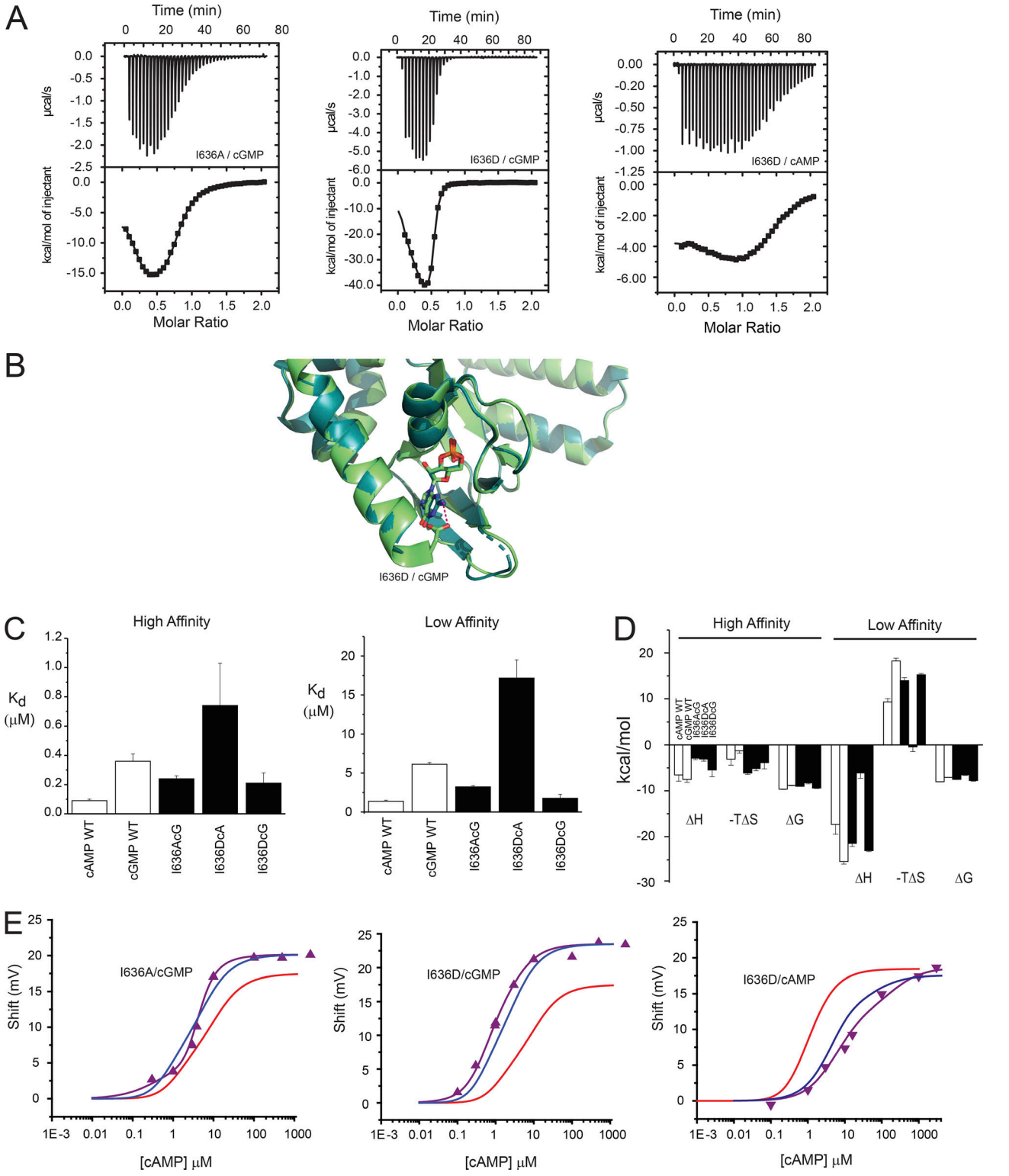

Figure 6. **Isoleucine 636 in the C-helix of the HCN2 C-terminus contributes to cAMP selectivity over cGMP. (A)** Plots of heat produced by progressive injections of cAMP or cGMP to the 200 µM mutant HCN2 C-terminus. The inflections in the top plot arise from injections of cyclic nucleotide, where the inverted peaks show the heat difference between the sample and reference compartment. The peaks decrease in magnitude as binding sites become saturated. The lower plots show values determined by integration of the area under the peaks from the upper plot versus the ratio of injected ligand to protein. The solid line through the values represents a two-site independent binding site model, which yielded values for affinity and energetics (ΔG, ΔH, and ΔS). **(B)** A ribbon diagram showing the CNBD of either wild type (I636, dark teal) or mutant (I636D, light green) bound to cGMP. Note that the aspartate residue forms a contact with the guanine ring of cGMP in the mutant, but not wild-type, structure. Residues distal to R635 (including I636) are not resolved in the cGMP-bound wild-type structure, whereas residues distal to D636 are not resolved in the cGMP-bound mutant structure. PDB accession no. 1Q3E (cGMP bound to wild type) and PDB accession no. 2Q0A (cGMP bound to mutant). The new hydrogen bond made by the aspartate side chain with 2-NH2 of cGMP is shown in magenta. **(C)** Bar

graphs of high- and low-affinity binding values that arise from the fitting of the heat values with a two-site independent binding model for the binding of cAMP and cGMP to the wild-type HCN2 C-terminus, cGMP binding to the I636A mutant, and cAMP and cGMP binding to the I636D mutant. Values for binding affinity are given in Table 1. **(D)** Bar graphs of values for thermodynamics that arise from the fitting of the heat values with a two-site independent binding model for the binding of cAMP and cGMP to the wild-type HCN2 C-terminus, cGMP binding to the I636A mutant, and cAMP and cGMP binding to the I636D mutant. Values in C and D represent means ± SEM. Each mean was determined from independent ITC binding experiments. **(E)** Concentration–response data and theoretical curves for the shift in gating produced by cAMP or cGMP to the 200-µM wild-type and mutant HCN2 C-terminus. The solid red line in the left and middle panels is the theoretical curve produced by the model that is fitted through the cGMP wild-type concentration–response data (from Fig. 6). The solid red line in the right panel is the theoretical curve produced by the model that is fitted through the cAMP wild-type concentration–response data (from Fig. 2). The solid blue lines are theoretical curves produced by the model using the experimental binding data obtained by ITC for the corresponding HCN2 mutant and using the gating parameters for the effect of cGMP (left and middle panels) or for cAMP (right panel) on the wild-type HCN2 channel. The purple triangles represent the concentration–response data for the effect of cGMP (left and middle panel) or the effect of cAMP (right panel) on the shift in the activation curve of the corresponding full-length mutant HCN2 channel. Note that the blue lines overlie closely with the experimental data (purple triangles), which are shifted to the left of the wild-type concentration–response data for cGMP (left and middle panel) and to the right of the wild-type concentration–response data for cAMP (right panel). The solid purple line represents a fit of the model to the mutant concentration–response data (purple triangles), which was made by adjusting the closed-to-open gating transitions.

substitution could be explained mainly by an enhancement of binding affinity.

By ITC, cAMP binding to the I636D mutant protein also yielded a pattern in the released heat that was well fitted with a two-independent binding site model (Fig. 6 A). In contrast to the binding affinity for cGMP, the binding affinity for cAMP was considerably decreased by the I636D mutation (Fig. 6 C and Table 1). The opposite effects of this mutation on cAMP and cGMP binding are consistent with the notion that this location in the wild-type channel is important for selecting cAMP over cGMP. Interestingly, although the thermodynamic signature for cAMP binding to the I636D mutant protein was similar to that for cAMP binding (and cGMP binding) to the wild-type protein (Fig. 6 D), the change in entropy for the low-affinity binding was very small and, unlike most other low-affinity binding events measured in this study, not unfavorable. Nevertheless, the free energy of cAMP binding for this mutant was still reduced for low-affinity binding, compared with cAMP and cGMP binding to the wild-type protein, because of the smaller change in favorable enthalpy.

We next examined how the changes in cAMP binding contribute to the differences in the concentration–response curves (Fig. 6 E). We introduced the cAMP binding affinities determined for the I636D mutant into the model without changing the closed-to-open transitions for the wild-type channel response to cAMP. Here, too, the theoretical curve closely follows the experimental data, which are shifted to the right of the concentration–response data for cAMP binding to the wild-type protein. Changes in the cAMP concentration–response curve induced by the aspartate substitution could be explained mainly by an enhancement of binding affinity. Thus, the data collected using the aspartate-substituted HCN2 channel, like those obtained from the alanine-substituted channel, suggest that I636 promotes selectivity of cAMP over cGMP mainly by augmenting cAMP binding affinity and gating, and by reducing cGMP binding affinity.

An increase in the height of the experimental cGMP data for both the I636A and I636D mutants compared with the wild type was not predicted by the mathematical model. The larger values of q for cGMP binding to those two mutants were chosen to fit the theoretical curve to the larger maximum effect as measured by experiment. We did this to make the comparison of the position of the theoretical and experimental curves along the x-axis easier to visualize. Thus, adjusting q was used as a tool to relate the change in open probability to the maximum shift in voltage. It may well be that there is a biological link between these, but we have not probed that more deeply here. Together with the small differences in shape or position between the experimental and theoretical curves, the small increase in height suggests that these mutations modestly promote the action of cGMP on gating, but how this occurs is not clear. Finally, we did not have values of q measured specifically for these two mutant channels by experiment.

The role of PBC and other C-helix residues in cGMP binding

We also examined the role of R591 and T592, in the PBC, on cGMP binding by substituting each residue with alanine. The positions of these two residues in the HCN2 structure, bound to cGMP, are shown in Fig. 7 A. Notably, a hydrogen bond is formed between the N2 atom of cGMP and T592 that is not observed in the cAMP-bound structure (Zagotta et al., 2003). Unlike cAMP binding to the two mutant HCN2 fragments, the heat released by cGMP binding was best fitted with a single-site independent binding model (Fig. 7 B). Again, this suggests a lack of negative cooperativity, or that any negative cooperativity is too small to be resolved.

We also examined three other residues in the C-helix that had a significant impact on cGMP binding. In Fig. 7 A, the positions of L633 and R635 are shown, whereas K638 was not resolved in the cGMP-bound structure. cGMP binding to L633A, R635A, and K638A mutant proteins produced heat values that were fitted best with only a single-site independent binding model, and thus lacked negative cooperativity (Fig. 7 B). Individual alanine substitutions of these residues reduced binding affinity but not to the same extent as R591A or T592A (Fig. 7 C and Table 1). Thus, the side chains from these three residues appear to be important for tight cGMP binding and negative cooperativity.

Two other residues of the C-helix, D631 and D634, were found to have smaller contributions to binding affinity of cGMP and their locations are shown in Fig. 8 A. cGMP binding to D631A and D634A mutant proteins produced heat values that were well fitted with a two-site independent binding model (Fig. 8 B). The values for K_d (Fig. 8 C and Table 1) and the thermodynamics of binding (Fig. 8 D) were not greatly altered by these

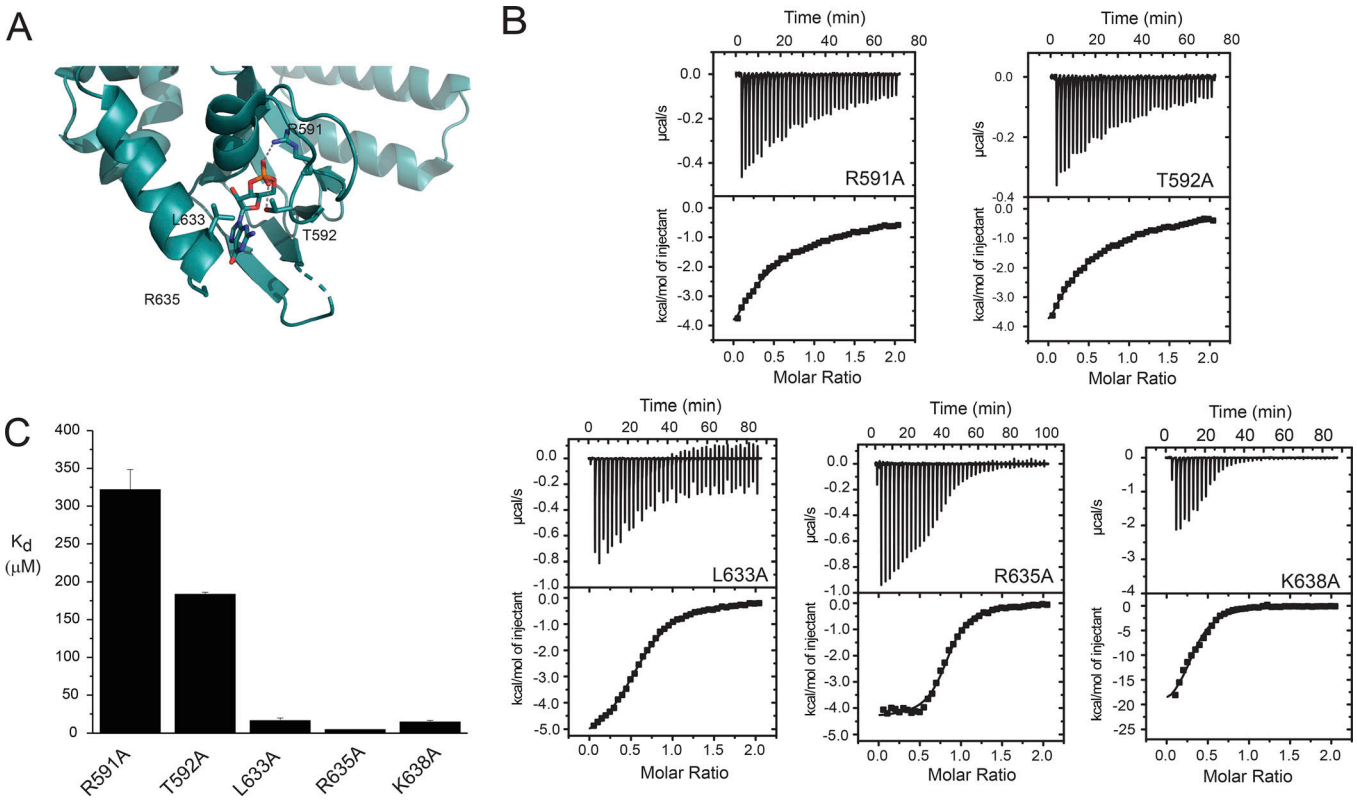

Figure 7. **Two residues in the PBC and three other residues in the C-helix make strong contributions to cGMP binding to the tetrameric HCN2 C-terminus. (A)** A ribbon diagram showing the wild-type HCN2 C-linker and CNBD bound to cGMP. The positions of R591 and T592, in the PBC, and L633A and R635, in the distal part of the C-helix, are shown. Residues distal to R635 (including K638) were not resolved in this structure. PDB accession no. 1Q3E. **(B)** Plots of heat produced upon progressive injections of cGMP to 200 µM HCN2 C-terminus wild-type or mutant proteins as measured by ITC. The inflections in the top plot arise from injections of cGMP, where each inverted peak shows the heat difference between the sample and reference compartment. The peaks decrease in magnitude as binding sites become saturated. The lower plot shows values determined by integration of the area under the peaks from the upper plot versus the ratio of injected ligand to protein. The solid line through the values represents a single binding site model, which yielded values for affinity and energetics (ΔG, ΔH, and ΔS). **(C)** A bar plot of values for the single affinity binding of cGMP to the tetrameric HCN2 C-terminal wild-type protein and mutants containing single mutations, from the experiments shown in A. Values represent means ± SEM. Each mean was determined from independent ITC binding experiments. Values for binding affinity are also shown in Table 1.

substitutions, which was also the case for the EC_{50} values determined by the Hill equation in a previous study (Zhou and Siegelbaum, 2007). The values for K_d were a bit lower and a bit higher for the D631A and D634A mutant proteins, respectively, than those for the wild-type protein. Thus, these aspartate residues, which make little contribution to cAMP binding affinity, also make small contributions to cGMP binding affinity. The small effects of these two mutations on cAMP and cGMP binding affinity suggest that the strength of binding and negative cooperativity is controlled by specific interactions between the binding site and the ligand.

Finally, we examined how R632 and E582 influence cGMP binding, which are found in the C-helix and PBC, respectively. As mentioned above, these proteins were purified with an HMT tag on the N-terminus, as they could not be purified in high enough amounts to assess binding after cleaving the HMT tag. Here, we also found that cGMP binding to the E582A-HMT protein produced a pattern of heat release that was best fitted with a single-site independent binding model and yielded a K_d of 690 µM for one trial (Fig. S1). In two trials, binding of cGMP to R632A-HMT protein was not detected (not depicted). These data support a critical role for these two residues in controlling potency (E582) and efficacy (R632) as suggested previously using full-length channels (Zhou and Siegelbaum, 2007).

Discussion

In this study, we developed a model for cAMP binding and the cAMP-induced depolarizing shift in the activation curve for the HCN2 channel using binding affinities obtained from a tetrameric C-terminal region of the channel and determined by ITC, and gating data for the full-length channel obtained from the literature. This model was developed by subsequent fitting to concentration–response data for channels containing one, two, three, and four binding sites, in that order, to constrain the selection of parameters for opening and closing. This model recapitulates the concentration–response curve for the effect of cAMP and cGMP on wild-type HCN2 channel opening, which bind with different affinity and also impact the opening differently. Notably, the model also predicts the concentration–response data in a subset of full-length channels with single amino acid substitutions in the binding site using only the

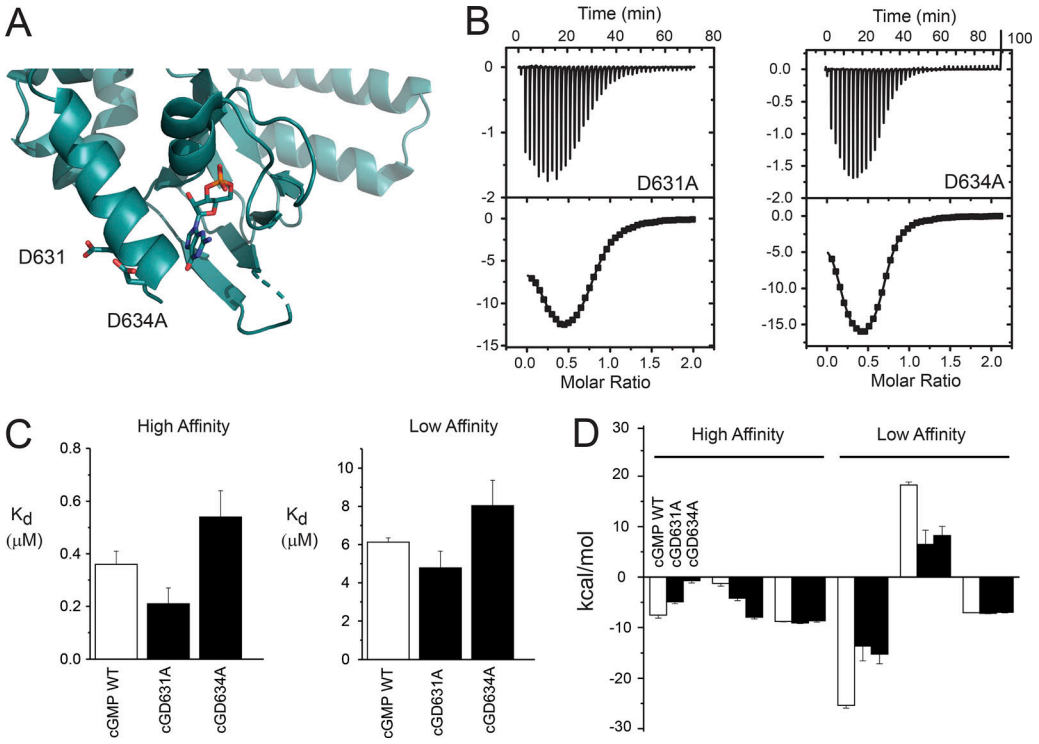

Figure 8. **Two aspartate residues in the distal C-helix make smaller contributions to cGMP binding to the tetrameric HCN2 C-terminus. (A)** A ribbon diagram showing the wild-type HCN2 C-linker and CNBD bound to cGMP. The positions of D631 and D634 in the distal part of the C-helix are shown. Residues distal to R635 (including K638) were not resolved in this structure. PDB accession no. 1Q3E. **(B)** Plots of heat produced upon progressive injections of cGMP to 200 µM HCN2 C-terminus, measured by ITC. The inflections in the top plot arise from injections of cGMP, where each inverted peak shows the heat difference between the sample and reference compartment. The peaks decrease in magnitude as binding sites become saturated. The lower plot shows values determined by integration of the area under the peaks from the upper plot versus the ratio of injected ligand to protein. The solid line through the values represents a two-site independent binding model, which yielded values for affinity and energetics (ΔG, ΔH, and ΔS). **(C)** Bar graphs of high- and low-affinity binding values that arise from the fitting of the heat values with a two-site independent binding model for the binding of cGMP to the tetrameric HCN2 C-terminal wild-type protein and mutants containing single mutations, from the experiments shown in A. Values for binding affinity are from Table 1. **(D)** Bar graphs of values for thermodynamics that arise from the fitting of the heat values with a two-site independent binding model for the binding of cGMP to the wild-type and mutant HCN2 C-terminus. Values in C and D represent means ± SEM. Each mean was determined from independent ITC binding experiments.

corresponding mutant experimental binding values and without altering wild type gating parameters of the liganded channel. Other mutants also appear to modestly affect the closed-to-open transitions of the liganded channel, which were adjusted to obtain appropriate fits. Thus, the results suggest that the cyclic nucleotide sensitivity of the HCN2 channel is determined by negatively cooperative binding affinity and allosteric effects on channel structure and opening, which are tuned by ligand-specific interactions and residues within the binding site.

Our measurements of binding by ITC were performed on a naturally occurring tetramer consisting of the C-linker and CNBD of the HCN2 C-terminus (Zagotta et al., 2003; Chow et al., 2012). The excellent agreement between our binding data and previously obtained functional measures of ligand sensitivity by patch-clamp electrophysiology in excised patches, which include mutations that both inhibit and augment both ligand binding and channel sensitivity (Zhou and Siegelbaum, 2007), provides strong evidence that the structure of the binding site and alterations in structure and dynamics induced by cAMP and cGMP binding to the tetrameric protein in solution reflect those that occur in the full-length channel in the plasma membrane. These data also suggest that the effect of mutations in the binding site on cAMP potency, which otherwise do not affect gating in the absence of ligand, can be estimated by the determination of binding affinities from ITC measurements on the appropriate tetrameric HCN2 C-terminus and using our model.

The binding of cAMP and cGMP to the wild-type HCN2 protein, and to most single-residue mutants, was well described by a two-site independent binding model that indicates negative cooperativity (see also the summary of binding affinities obtained in Fig. S2). We have shown this pattern of binding for the HCN2 tetramer as well as for the equivalent HCN4 tetrameric protein (Chow et al., 2012; Ng et al., 2016), and this has since been reported in a more recent study of HCN4 (Hayoz et al., 2017). The high-affinity events were associated with favorable entropy and favorable enthalpy, whereas the lower-affinity events were associated with favorable enthalpy but entropy that is unfavorable (see also the summary of thermodynamic values in Fig. S3). The enthalpic component of low-affinity binding is even larger than that for high-affinity binding, and therefore, the thermodynamic basis for negative cooperativity is entirely entropic. Based on this thermodynamic signature, we

suspect that high-affinity ligand binding may be associated with distinct and more modest alterations in structure that are normally associated with enthalpy, e.g., alterations in the mean backbone conformation, as well as with alterations that are associated with favorable changes in entropy. This has been suggested for other proteins including the dimeric catabolite activating protein, which also binds cAMP and contains a CNBD that is similar to that in HCN channels (Cooper and Dryden, 1984; Popovych et al., 2006; Cui and Karplus, 2008; Kalodimos, 2012).

Further information on the nature of cAMP binding to HCN2 comes from an analysis of heat capacity (ΔC_p), which is the amount of heat required to increase the temperature of a system by 1 degree Kelvin. Heat capacity can be estimated by measuring ΔH as a function of temperature by ITC and calculating the slope of the resulting relationship (Boudker and Oh, 2015). Using data collected from our previous study, we plotted ΔH for the high- and low-affinity binding of cAMP to the wild-type HCN2 C-terminal tetramer at 10°C and 25°C (Fig. 9). Assuming that the relationship of ΔH is linear as a function of temperature, the calculated values for ΔC_p are −159 cal/mol/°C and −898 cal/mol/°C for the high- and low-affinity binding events, respectively. The difference in heat capacity between these binding events suggests that the underlying changes in the ligand protein complex are different. Together with the other thermodynamic measures from ITC, the difference in heat capacity supports a model where high-affinity binding is associated with distinct alterations in structure compared with low-affinity binding.

Support for the intermediately liganded and fully liganded channel having distinct alterations in structure also comes from previous electrophysiological experiments. In the HCN2 channel, cAMP and cGMP produce an increase in maximum current as well as a shift in the channel activation curve (Craven and Zagotta, 2004; Zhou and Siegelbaum, 2007), on which we focused in the current study. For cAMP and cGMP, concentration–response curves revealed that the EC_{50} was less for the increase in maximum current, indicative of greater sensitivity, than it was for the shift in current activation by voltage (Zhou and Siegelbaum, 2007). This finding is supported by Kusch et al. (2010), who showed that the increase in maximum current saturates at lower levels of cAMP than those required to saturate the depolarizing shift in channel activation, possibly after only two of four sites are occupied. The same authors, using a fluorescent cAMP molecule to estimate binding affinity in the full-length HCN2 channel, also suggested that cAMP binds with negative cooperativity to the full-length HCN2 channel, although the decrease in affinity is much larger than what we had found by ITC (Chow et al., 2012), and it occurred upon cAMP binding to the second site (Kusch et al., 2011). Finally, alanine substitution of arginine 632 (R632A; in the C-helix) eliminated the depolarizing shift in channel activation produced by cAMP and cGMP, but the increase in maximum current remained (Zhou and Siegelbaum, 2007), which supports distinct molecular mechanisms for each. This increase in maximum current was eliminated by the R591E mutation (charge reversal in the canonical CNBD), performed in the background of R632A, which confirmed that this increase was not due to cAMP bound to a separate site. Together, these data are consistent with a model whereby high-affinity binding of cAMP is associated with alterations in structure and function that are distinct from those produced by low-affinity binding.

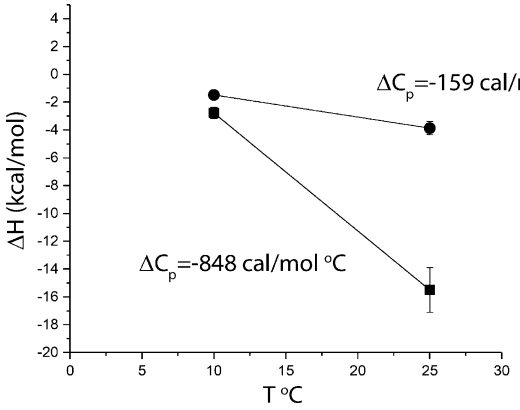

Figure 9. **The calculated heat capacity for the high-affinity binding of cAMP to the tetrameric HCN2 C-terminus is smaller than that for low-affinity binding.** A graph showing the values for ΔH calculated at 25°C (black squares) and 10°C (black circles), which were determined in a previous study by our group (Chow et al., 2012). The calculated slopes yield heat capacity and are shown next to their respective relation in the graph. Values represent means ± SEM.

Further support for this asymmetric model, and a possible molecular mechanism for partial agonism, comes from our previous experiments using cIMP and cCMP (Ng et al., 2016), which had been shown to act as a partial agonist of the HCN2 and the sinoatrial HCN channels (DiFrancesco and Tortora, 1991; Zong et al., 2012). We found that these partial agonists did not bind to the tetrameric HCN2 C-terminus (at 200 µM) with negative cooperativity but that the thermodynamic signature was similar to the high-affinity binding event for cAMP and other "full" agonists. Also, unlike cAMP, cCMP and cIMP were not able to promote tetramerization of low concentrations (10 and 25 µM) of the HCN2 C-terminus, even when these cyclic nucleotides were present at very high levels, which suggests that ligand-induced tetramer formation occurs in concert with low-affinity binding and not with high-affinity binding. These data, together with our model, suggest that (a) partial agonism arises because cCMP and cIMP may not be able to bind to the low-affinity site even when present at very high levels or, if they do bind to the low-affinity site, do not reproduce the downstream effects of full agonists, and (b) binding to the high-affinity site by cCMP and cIMP may induce intersubunit interactions that are distinct from those induced by cAMP and other full agonists. This mechanism for partial agonism is similar to the half-of-sites reactivity that has been proposed for enzymes, a limiting case of negative cooperativity where the subunits may never be fully occupied (Levitzki and Koshland, 1976). An inability to bind a low-affinity site may be due to the nature of the partial agonist itself and/or the induction of a distinct state of the low-affinity site by the partial agonist with an even lower binding affinity than those induced by cAMP or cGMP. The latter scenario is supported by our finding that some of the single mutations had larger effects on either the high- or low-affinity binding (Fig. S2,

B and D). These data imply that changes occurring upon high-affinity binding depend on interactions between the binding site and the ligand and, furthermore, that specific ligands may tune negative cooperativity, and ligand sensitivity, by promoting low-affinity binding sites with distinct affinities.

cAMP is a more potent facilitator of opening than cGMP in the HCN2 channel as well as in HCN channels in the sinoatrial node of the heart, but the maximum effect is similar between the two ligands (DiFrancesco and Tortora, 1991; Zagotta et al., 2003; Zhou and Siegelbaum, 2007). We used the model to compare the potency of cAMP and cGMP on HCN2 channel opening, and to determine why they are different. The model did not predict the concentration–response curve for cGMP when the experimentally determined binding affinities for cGMP were used in conjunction with the gating parameters determined for cAMP; this resulted in a curve that was shifted to lower concentrations of cGMP, and that was to the left of, and steeper than, the experimental concentration–response curve. To fit the experimental concentration–response curve precisely, changes to the closed to open transitions also had to be made. Thus, our analysis suggests that the more potent facilitation by cAMP is due to stronger effects on the closed to open transitions as well as to its greater binding affinity and as compared with cGMP. A similar suggestion was made in a recent study on the SthK (Schmidpeter et al., 2018), a CNG channel from *Spirochaeta thermophila* that is structurally and evolutionarily related to the HCN channels (Brams et al., 2014; Kesters et al., 2015), which showed that cGMP binds with an affinity that is similar to cAMP but that it opens the channel less efficiently. Structures of the HCN2 channel show that cGMP binds in the *syn* configuration whereas cAMP binds in the *anti* configuration, and that each ligand makes unique interactions within the binding site (Zagotta et al., 2003). The unique interactions made by them are likely responsible for the differences in both binding affinity and gating effects. Indeed, recent studies using ^{15}N-transverse relaxation optimized spectroscopy NMR, double electron-electron resonance, and single-molecule fluorescence on the HCN2 C-terminus suggest that allosteric mechanisms of cAMP and cGMP are different even though their effects on pore opening may be similar (DeBerg et al., 2016; Goldschen-Ohm et al., 2017). The larger fold difference between low- and high-affinity binding, for cAMP compared with cGMP, found here (3.4-fold and 3-fold, respectively) and previously found by us (3.7-fold vs. 2.3-fold, respectively; Ng et al., 2016) also suggests that the interactions made by them in the binding site are distinct from each other. Thus, cAMP may also promote negative cooperativity to a greater extent than cGMP, which would impact the difference in the concentration–response relation. Nevertheless, as we reported previously (Ng et al., 2016), the affinity for cGMP seems low enough (<0.4 µM for the high-affinity binding event) that binding could potentially occur normally in vivo, especially under conditions where the intracellular levels of cAMP are low.

In summary, we found that the potency of the cyclic nucleotide–mediated shift of channel activation to more negative voltages can be explained and predicted by a mathematical model of opening that incorporates negatively cooperative binding. Our binding data, measured by ITC, also yield thermodynamic information on the underlying molecular and atomic mechanisms, and they support asymmetric and distinct alterations in structure in response to cyclic nucleotide binding. Most of the experiments that have examined the effects of cyclic nucleotide binding on alterations in structure focused on the monomeric bound and unbound C-terminal protein (e.g., Taraska et al., 2009; Möller et al., 2014; Goldschen-Ohm et al., 2016) or report on the apo and/or fully liganded state of HCN C-terminal or full-length tetramers (e.g., Zagotta et al., 2003; Lolicato et al., 2011; Lee and MacKinnon, 2017). We suspect that solved structures for the intermediately liganded HCN2 channel, which have yet to be obtained, may demonstrate distinct alterations that reflect the binding of cAMP and cGMP mainly to a high-affinity site, as has been shown in other negatively cooperative proteins (Koshland, 1996; Stevens et al., 2001; Popovych et al., 2006). Likewise, we suspect that solved structures of the HCN2 channel bound to partial agonists may also be distinct from those either partly or completely bound to full agonists such as cAMP or cGMP. Such structures would provide critical insight into the underlying molecular process by which cyclic nucleotides facilitate channel opening.

Acknowledgments

Merritt C. Maduke served as editor.

This work was supported by operating funds from the Canadian Institutes of Health Research (MOP-106655) and the Natural Sciences and Engineering Research Council of Canada (RGPIN-203288) to E.A. Accili. E.A. Accili is also a recipient of a Tier II Canada Research Chair, and M. Zhuang is a recipient of a Natural Sciences and Engineering Research Council of Canada Undergraduate Student Research Award.

The authors declare no competing financial interests.

Author contributions: L.C.T. Ng and E.A. Accili designed the study, with feedback from F. Van Petegem. L.C.T. Ng and M. Zhuang conducted the experiments, analyzed and interpreted the experimental data, and prepared the associated figures. E.A. Accili and F. Van Petegem also helped to interpret the experimental data and its analysis.Y.X. Li developed the mathematical model in collaboration with E.A. Accili and L.C.T. Ng, who also prepared the associated figures L.C.T. Ng and E.A. Accili wrote the manuscript, which was reviewed and edited by all of the authors.

Submitted: 20 June 2018
Revised: 26 April 2019
Accepted: 31 July 2019

References

Akimoto, M., Z. Zhang, S. Boulton, R. Selvaratnam, B. VanSchouwen, M. Gloyd, E.A. Accili, O.F. Lange, and G. Melacini. 2014. A mechanism for the auto-inhibition of hyperpolarization-activated cyclic nucleotide-gated (HCN) channel opening and its relief by cAMP. *J. Biol. Chem.* 289:22205–22220. https://doi.org/10.1074/jbc.M114.572164

Akimoto, M., B. VanSchouwen, and G. Melacini. 2018. The Structure of the Apo cAMP-Binding Domain of HCN4: A Stepping Stone towards Understanding the cAMP-Dependent Modulation of the Hyperpolarization-Activated

Cyclic-Nucleotide-Gated (HCN) Ion Channels. *FEBS J.* 285:2182–2192. https://doi.org/10.1111/febs.14408

Boudker, O., and S. Oh. 2015. Isothermal titration calorimetry of ion-coupled membrane transporters. *Methods.* 76:171–182. https://doi.org/10.1016/j.ymeth.2015.01.012

Brams, M., J. Kusch, R. Spurny, K. Benndorf, and C. Ulens. 2014. Family of prokaryote cyclic nucleotide-modulated ion channels. *Proc. Natl. Acad. Sci. USA.* 111:7855–7860. https://doi.org/10.1073/pnas.1401917111

Chen, S., J. Wang, and S.A. Siegelbaum. 2001. Properties of hyperpolarization-activated pacemaker current defined by coassembly of HCN1 and HCN2 subunits and basal modulation by cyclic nucleotide. *J. Gen. Physiol.* 117:491–504. https://doi.org/10.1085/jgp.117.5.491

Chow, S.S., F. Van Petegem, and E.A. Accili. 2012. Energetics of cyclic AMP binding to HCN channel C terminus reveal negative cooperativity. *J. Biol. Chem.* 287:600–606. https://doi.org/10.1074/jbc.M111.269563

Christensen, A.E., F. Selheim, J. de Rooij, S. Dremier, F. Schwede, K.K. Dao, A. Martinez, C. Maenhaut, J.L. Bos, H.G. Genieser, and S.O. Døskeland. 2003. cAMP analog mapping of Epac1 and cAMP kinase. Discriminating analogs demonstrate that Epac and cAMP kinase act synergistically to promote PC-12 cell neurite extension. *J. Biol. Chem.* 278:35394–35402. https://doi.org/10.1074/jbc.M302179200

Colquhoun, D. 1998. Binding, gating, affinity and efficacy: the interpretation of structure-activity relationships for agonists and of the effects of mutating receptors. *Br. J. Pharmacol.* 125:924–947. https://doi.org/10.1038/sj.bjp.0702164

Cooper, A., and D.T. Dryden. 1984. Allostery without conformational change. A plausible model. *Eur. Biophys. J.* 11:103–109. https://doi.org/10.1007/BF00276625

Craven, K.B., and W.N. Zagotta. 2004. Salt bridges and gating in the COOH-terminal region of HCN2 and CNGA1 channels. *J. Gen. Physiol.* 124:663–677. https://doi.org/10.1085/jgp.200409178

Cui, Q., and M. Karplus. 2008. Allostery and cooperativity revisited. *Protein Sci.* 17:1295–1307. https://doi.org/10.1110/ps.03259908

Das, R., V. Esposito, M. Abu-Abed, G.S. Anand, S.S. Taylor, and G. Melacini. 2007. cAMP activation of PKA defines an ancient signaling mechanism. *Proc. Natl. Acad. Sci. USA.* 104:93–98. https://doi.org/10.1073/pnas.0609033103

DeBerg, H.A., P.S. Brzovic, G.E. Flynn, W.N. Zagotta, and S. Stoll. 2016. Structure and Energetics of Allosteric Regulation of HCN2 Ion Channels by Cyclic Nucleotides. *J. Biol. Chem.* 291:371–381. https://doi.org/10.1074/jbc.M115.696450

DiFrancesco, D., and P. Tortora. 1991. Direct activation of cardiac pacemaker channels by intracellular cyclic AMP. *Nature.* 351:145–147. https://doi.org/10.1038/351145a0

Flynn, G.E., K.D. Black, L.D. Islas, B. Sankaran, and W.N. Zagotta. 2007. Structure and rearrangements in the carboxy-terminal region of SpIH channels. *Structure.* 15:671–682. https://doi.org/10.1016/j.str.2007.04.008

Gauss, R., R. Seifert, and U.B. Kaupp. 1998. Molecular identification of a hyperpolarization-activated channel in sea urchin sperm. *Nature.* 393:583–587. https://doi.org/10.1038/31248

Goldschen-Ohm, M.P., V.A. Klenchin, D.S. White, J.B. Cowgill, Q. Cui, R.H. Goldsmith, and B. Chanda. 2016. Structure and dynamics underlying elementary ligand binding events in human pacemaking channels. *eLife.* 5:e20797. https://doi.org/10.7554/eLife.20797

Goldschen-Ohm, M.P., D.S. White, V.A. Klenchin, B. Chanda, and R.H. Goldsmith. 2017. Observing Single-Molecule Dynamics at Millimolar Concentrations. *Angew. Chem. Int. Ed. Engl.* 56:2399–2402. https://doi.org/10.1002/anie.201612050

Goulding, E.H., G.R. Tibbs, and S.A. Siegelbaum. 1994. Molecular mechanism of cyclic-nucleotide-gated channel activation. *Nature.* 372:369–374. https://doi.org/10.1038/372369a0

Hayoz, S., P.B. Tiwari, G. Piszczek, A. Üren, and T.I. Brelidze. 2017. Investigating cyclic nucleotide and cyclic dinucleotide binding to HCN channels by surface plasmon resonance. *PLoS One.* 12:e0185359. https://doi.org/10.1371/journal.pone.0185359

Hines, K.E., T.R. Middendorf, and R.W. Aldrich. 2014. Determination of parameter identifiability in nonlinear biophysical models: A Bayesian approach. *J. Gen. Physiol.* 143:401–416. https://doi.org/10.1085/jgp.201311116

Idikuda, V., W. Gao, Z. Su, Q. Liu, and L. Zhou. 2019. cAMP binds to closed, inactivated, and open sea urchin HCN channels in a state-dependent manner. *J. Gen. Physiol.* 151:200–213. https://doi.org/10.1085/jgp.201812019

Jackson, H.A., C.R. Marshall, and E.A. Accili. 2007. Evolution and structural diversification of hyperpolarization-activated cyclic nucleotide-gated channel genes. *Physiol. Genomics.* 29:231–245. https://doi.org/10.1152/physiolgenomics.00142.2006

Kalodimos, C.G. 2012. Protein function and allostery: a dynamic relationship. *Ann. N. Y. Acad. Sci.* 1260:81–86. https://doi.org/10.1111/j.1749-6632.2011.06319.x

Kesters, D., M. Brams, M. Nys, E. Wijckmans, R. Spurny, T. Voets, J. Tytgat, J. Kusch, and C. Ulens. 2015. Structure of the SthK carboxy-terminal region reveals a gating mechanism for cyclic nucleotide-modulated ion channels. *PLoS One.* 10:e0116369. https://doi.org/10.1371/journal.pone.0116369

Koshland, D.E. Jr. 1996. The structural basis of negative cooperativity: receptors and enzymes. *Curr. Opin. Struct. Biol.* 6:757–761. https://doi.org/10.1016/S0959-440X(96)80004-2

Kusch, J., C. Biskup, S. Thon, E. Schulz, V. Nache, T. Zimmer, F. Schwede, and K. Benndorf. 2010. Interdependence of receptor activation and ligand binding in HCN2 pacemaker channels. *Neuron.* 67:75–85. https://doi.org/10.1016/j.neuron.2010.05.022

Kusch, J., S. Thon, E. Schulz, C. Biskup, V. Nache, T. Zimmer, R. Seifert, F. Schwede, and K. Benndorf. 2011. How subunits cooperate in cAMP-induced activation of homotetrameric HCN2 channels. *Nat. Chem. Biol.* 8:162–169. https://doi.org/10.1038/nchembio.747

Leavitt, S., and E. Freire. 2001. Direct measurement of protein binding energetics by isothermal titration calorimetry. *Curr. Opin. Struct. Biol.* 11:560–566. https://doi.org/10.1016/S0959-440X(00)00248-7

Lee, C.H., and R. MacKinnon. 2017. Structures of the Human HCN1 Hyperpolarization-Activated Channel. *Cell.* 168:111–120.e111. https://doi.org/10.1016/j.cell.2016.12.023

Levitzki, A., and D.E. Koshland Jr. 1976. The role of negative cooperativity and half-of-the-sites reactivity in enzyme regulation. *Curr. Top. Cell. Regul.* 10:1–40. https://doi.org/10.1016/B978-0-12-152810-2.50008-5

Lolicato, M., M. Nardini, S. Gazzarrini, S. Möller, D. Bertinetti, F.W. Herberg, M. Bolognesi, H. Martin, M. Fasolini, J.A. Bertrand, et al. 2011. Tetramerization dynamics of C-terminal domain underlies isoform-specific cAMP gating in hyperpolarization-activated cyclic nucleotide-gated channels. *J. Biol. Chem.* 286:44811–44820. https://doi.org/10.1074/jbc.M111.297606

Ludwig, A., X. Zong, M. Jeglitsch, F. Hofmann, and M. Biel. 1998. A family of hyperpolarization-activated mammalian cation channels. *Nature.* 393:587–591. https://doi.org/10.1038/31255

Matulef, K., and W.N. Zagotta. 2002. Multimerization of the ligand binding domains of cyclic nucleotide-gated channels. *Neuron.* 36:93–103. https://doi.org/10.1016/S0896-6273(02)00878-4

Matulef, K., G.E. Flynn, and W.N. Zagotta. 1999. Molecular rearrangements in the ligand-binding domain of cyclic nucleotide-gated channels. *Neuron.* 24:443–452. https://doi.org/10.1016/S0896-6273(00)80857-0

Mazzolini, M., M. Punta, and V. Torre. 2002. Movement of the C-helix during the gating of cyclic nucleotide-gated channels. *Biophys. J.* 83:3283–3295. https://doi.org/10.1016/S0006-3495(02)75329-0

Möller, S., A. Alfieri, D. Bertinetti, M. Aquila, F. Schwede, M. Lolicato, H. Rehmann, A. Moroni, and F.W. Herberg. 2014. Cyclic nucleotide mapping of hyperpolarization-activated cyclic nucleotide-gated (HCN) channels. *ACS Chem. Biol.* 9:1128–1137. https://doi.org/10.1021/cb400904s

Ng, L.C.T., I. Putrenko, V. Baronas, F. Van Petegem, and E.A. Accili. 2016. Cyclic Purine and Pyrimidine Nucleotides Bind to the HCN2 Ion Channel and Variably Promote C-Terminal Domain Interactions and Opening. *Structure.* 24:1629–1642. https://doi.org/10.1016/j.str.2016.06.024

Popovych, N., S. Sun, R.H. Ebright, and C.G. Kalodimos. 2006. Dynamically driven protein allostery. *Nat. Struct. Mol. Biol.* 13:831–838. https://doi.org/10.1038/nsmb1132

Puljung, M.C., and W.N. Zagotta. 2013. A secondary structural transition in the C-helix promotes gating of cyclic nucleotide-regulated ion channels. *J. Biol. Chem.* 288:12944–12956. https://doi.org/10.1074/jbc.M113.464123

Puljung, M.C., H.A. DeBerg, W.N. Zagotta, and S. Stoll. 2014. Double electron-electron resonance reveals cAMP-induced conformational change in HCN channels. *Proc. Natl. Acad. Sci. USA.* 111:9816–9821. https://doi.org/10.1073/pnas.1405371111

Santoro, B., D.T. Liu, H. Yao, D. Bartsch, E.R. Kandel, S.A. Siegelbaum, and G.R. Tibbs. 1998. Identification of a gene encoding a hyperpolarization-activated pacemaker channel of brain. *Cell.* 93:717–729. https://doi.org/10.1016/S0092-8674(00)81434-8

Saponaro, A., S.R. Pauleta, F. Cantini, M. Matzapetakis, C. Hammann, C. Donadoni, L. Hu, G. Thiel, L. Banci, B. Santoro, and A. Moroni. 2014. Structural basis for the mutual antagonism of cAMP and TRIP8b in regulating HCN channel function. *Proc. Natl. Acad. Sci. USA.* 111:14577–14582. https://doi.org/10.1073/pnas.1410389111

Schmidpeter, P.A.M., X. Gao, V. Uphadyay, J. Rheinberger, and C.M. Nimigean. 2018. Ligand binding and activation properties of the purified bacterial cyclic nucleotide-gated channel SthK. *J. Gen. Physiol.* 150: 821–834. https://doi.org/10.1085/jgp.201812023

Shabb, J.B., and J.D. Corbin. 1992. Cyclic nucleotide-binding domains in proteins having diverse functions. *J. Biol. Chem.* 267:5723–5726.

Stevens, S.Y., S. Sanker, C. Kent, and E.R. Zuiderweg. 2001. Delineation of the allosteric mechanism of a cytidylyltransferase exhibiting negative cooperativity. *Nat. Struct. Biol.* 8:947–952. https://doi.org/10.1038/nsb1101-947

Taraska, J.W., M.C. Puljung, N.B. Olivier, G.E. Flynn, and W.N. Zagotta. 2009. Mapping the structure and conformational movements of proteins with transition metal ion FRET. *Nat. Methods.* 6:532–537. https://doi.org/10.1038/nmeth.1341

Tibbs, G.R., D.T. Liu, B.G. Leypold, and S.A. Siegelbaum. 1998. A state-independent interaction between ligand and a conserved arginine residue in cyclic nucleotide-gated channels reveals a functional polarity of the cyclic nucleotide binding site. *J. Biol. Chem.* 273:4497–4505. https://doi.org/10.1074/jbc.273.8.4497

Ulens, C., and S.A. Siegelbaum. 2003. Regulation of hyperpolarization-activated HCN channels by cAMP through a gating switch in binding domain symmetry. *Neuron.* 40:959–970. https://doi.org/10.1016/S0896-6273(03)00753-0

Varnum, M.D., K.D. Black, and W.N. Zagotta. 1995. Molecular mechanism for ligand discrimination of cyclic nucleotide-gated channels. *Neuron.* 15: 619–625. https://doi.org/10.1016/0896-6273(95)90150-7

Velázquez Campoy, A., and E. Freire. 2005. ITC in the post-genomic era...? Priceless. *Biophys. Chem.* 115:115–124. https://doi.org/10.1016/j.bpc.2004.12.015

Velázquez-Campoy, A., H. Ohtaka, A. Nezami, S. Muzammil, and E. Freire. 2004. Isothermal titration calorimetry. *Curr. Protoc. Cell Biol.* Chapter 17: Unit 17.18.

Wainger, B.J., M. DeGennaro, B. Santoro, S.A. Siegelbaum, and G.R. Tibbs. 2001. Molecular mechanism of cAMP modulation of HCN pacemaker channels. *Nature.* 411:805–810. https://doi.org/10.1038/35081088

Wang, J., S. Chen, and S.A. Siegelbaum. 2001. Regulation of hyperpolarization-activated HCN channel gating and cAMP modulation due to interactions of COOH terminus and core transmembrane regions. *J. Gen. Physiol.* 118: 237–250. https://doi.org/10.1085/jgp.118.3.237

Weber, I.T., and T.A. Steitz. 1987. Structure of a complex of catabolite gene activator protein and cyclic AMP refined at 2.5 A resolution. *J. Mol. Biol.* 198:311–326. https://doi.org/10.1016/0022-2836(87)90315-9

Wiseman, T., S. Williston, J.F. Brandts, and L.N. Lin. 1989. Rapid measurement of binding constants and heats of binding using a new titration calorimeter. *Anal. Biochem.* 179:131–137. https://doi.org/10.1016/0003-2697(89)90213-3

Zagotta, W.N., N.B. Olivier, K.D. Black, E.C. Young, R. Olson, and E. Gouaux. 2003. Structural basis for modulation and agonist specificity of HCN pacemaker channels. *Nature.* 425:200–205. https://doi.org/10.1038/nature01922

Zhou, L., and S.A. Siegelbaum. 2007. Gating of HCN channels by cyclic nucleotides: residue contacts that underlie ligand binding, selectivity, and efficacy. *Structure.* 15:655–670. https://doi.org/10.1016/j.str.2007.04.012

Zong, X., S. Krause, C.C. Chen, J. Krüger, C. Gruner, X. Cao-Ehlker, S. Fenske, C. Wahl-Schott, and M. Biel. 2012. Regulation of hyperpolarization-activated cyclic nucleotide-gated (HCN) channel activity by cCMP. *J. Biol. Chem.* 287:26506–26512. https://doi.org/10.1074/jbc.M112.357129